



HAL
open science

Edging towards an understanding of CH/CH₂ on nano-diamonds

A. P. Jones

► **To cite this version:**

A. P. Jones. Edging towards an understanding of CH/CH₂ on nano-diamonds. *Astronomy & Astrophysics - A&A*, 2022, 657, pp.A127. 10.1051/0004-6361/202141792 . hal-03539682

HAL Id: hal-03539682

<https://hal.science/hal-03539682v1>

Submitted on 21 Jan 2022

HAL is a multi-disciplinary open access archive for the deposit and dissemination of scientific research documents, whether they are published or not. The documents may come from teaching and research institutions in France or abroad, or from public or private research centers.

L'archive ouverte pluridisciplinaire **HAL**, est destinée au dépôt et à la diffusion de documents scientifiques de niveau recherche, publiés ou non, émanant des établissements d'enseignement et de recherche français ou étrangers, des laboratoires publics ou privés.

Edging towards an understanding of CH/CH₂ on nano-diamonds

Regular and semi-regular polyhedra and diamond network models

A. P. Jones

Université Paris-Saclay, CNRS, Institut d'Astrophysique Spatiale, 91405, Orsay, France
e-mail: anthony.jones@universite-paris-saclay.fr

Received 14 July 2021 / Accepted 1 November 2021

ABSTRACT

Context. Nano-diamonds have been observed in only a handful of circumstellar regions 10–100 AU from moderately bright stars ($T_{\text{eff}} \sim 8000\text{--}10\,000$ K). They have also been extracted from primitive meteorites; some of these are clearly pre-solar, that is to say that they formed far from the solar system and therefore traversed the interstellar medium, where they must exist but, because we see no evidence of them, must be extremely well hidden.

Aims. Our goal is to understand if it is possible to constrain the sizes and shapes of nano-diamonds in circumstellar media using the observed ratio, [CH]/[CH₂], of their surface CH₂ and CH infrared bands at ≈ 3.43 μm and ≈ 3.53 μm , respectively.

Methods. We calculated the CH and CH₂ abundances on nano-diamonds using two approaches. The first assumes regular and semi-regular polyhedra (tetrahedra, octahedra, and cubes and their truncated forms). The second uses a diamond bonding network to derive the structures of tetrahedral and octahedral particles, and their truncated variants, and also of spherical nano-diamonds.

Results. As a function of the particle size and shape, and for the two different calculation methods, we derived the relative abundance ratio [CH]/[CH₂], which can then be weighted by their laboratory-measured infrared band intensities. The two methods give good agreement and indicate that the spread in values, over the different particle forms, is more than an order of magnitude for any size.

Conclusions. We conclude that the ratio [CH]/[CH₂], and their infrared band ratio, strongly depend upon particle size and shape. For a given shape or size, the ratio can vary by more than an order of magnitude. It may therefore be difficult to constrain nano-diamond sizes using the observed 3–4 μm spectra alone. *James Webb* Space Telescope mid-infrared spectra may help, but only if bands are size-specific.

Key words. dust, extinction – ISM: abundances

1. Introduction

Nano-diamonds with median radii of 1.3–1.5 nm (Daulton et al. 1996) have been extracted from meteorites in abundances of up to ≈ 1400 ppm (Huss & Lewis 1995). Their isotopically anomalous Xe content is considered characteristic of supernovae (Lewis et al. 1987), and their ¹⁵N depletion and low C/N ratios are typical of carbon-rich stellar environments (Alexander 1997). The observation of a CH stretching mode at 3.47 μm towards dense regions was originally thought to be an indicator of the presence of nano-diamonds in the interstellar medium (ISM) (Allamandola et al. 1992), but most likely has another origin (Brooke et al. 1996). However, we do today have conclusive observational evidence for the presence of nano-diamonds in proto-planetary discs where they are identified by their characteristic CH_{*n*} (*n* = 1, 2) stretching modes at 3.43 and 3.53 μm (e.g. Guillois et al. 1999; Van Kerckhoven et al. 2002; Habart et al. 2004).

In the laboratory, diamond-like materials and nano-diamonds have long been synthesised and studied and there exists a vast literature on this subject¹. In most of these laboratory studies, we have the luxury of being able to directly analyse the textures, particle sizes, and shapes through a myriad

of sophisticated techniques (e.g. scanning and tunnelling electron microscopy and atomic force microscopy). In astronomical observations this option is not available to us and so we must progress using solid-state material models. Our understanding is therefore critically constrained by the limitations of our knowledge and our models.

In order to model, analyse, and interpret the spectra of the nano-diamonds observed in circumstellar proto-planetary discs, we required well-determined wavelength- and size-dependent optical constants: the complex indices of refraction. These were then used to calculate the optical properties of nano-diamonds and thence their extinction, absorption, and scattering cross-sections, which in turn were used to derive their temperatures in a given stellar radiation field. In the following paper, we derive the nano-diamond optical constants and, in this paper, as a key input to this modelling, we concern ourselves with approximating nano-diamond structures using regular and semi-regular polyhedral shapes, principally tetrahedra (T) and octahedra (O), and their truncated forms (tT and tO), but also consider cuboctahedra (cO), cubes (C), and truncated cubes (tC). Additionally we developed a diamond bonding network model to derive the structures of tetrahedral and octahedral particles and their truncated forms.

A key question in unravelling the essential characteristics of the 3–4 μm infrared bands that have been attributed to nano-diamonds and, in particular the 3.53 μm /3.43 μm ratio, is how their size and the shape (e.g. rounded, angular, crystal-faceted

¹ Here we desist from giving any obviously limited and highly-selective citation of this literature.

[euهدral], ...) can affect this ratio. Here we consider this question from a purely geometrical aspect, that is by considering the surface and edge structures of euهدral forms modelled as regular polyhedra and diamond-bonded networks. The principal product of both of our nano-diamond modelling approaches is the relative abundance ratio $[\text{CH}]/[\text{CH}_2]$ of nano-diamonds as a function of the particle size and shape.

This paper is structured as follows: Sect. 2 describes the nano-diamond physical properties, Sect. 3 considers particle shapes and surfaces, Sect. 4 details the polyhedral methodology for a range of regular forms, Sect. 5 describes semi-regular truncated polyhedra, Sect. 6 presents the diamond-bonded network methodology, Sect. 7 discusses the predicted CH/CH₂ ratios in nano-diamonds and their use as a ruler, Sect. 8 considers nano-diamond stability and surface dehydrogenation effects, Sect. 9 discusses the implications of the results and speculates upon their utility, and Sect. 10 summarises the work and presents the conclusions.

2. Nano-diamond physical properties

The diagnostic potential of interstellar dust species is principally driven by their characteristic infrared spectra. In order to fully utilise this potential for hydro-carbonaceous dust, be it aliphatic-rich, aromatic-rich or (nano)diamond, we need to understand how the particle size, composition, and morphology determine its spectroscopic signatures. For nano-diamonds there is a wealth of laboratory data to aid us (e.g. Lewis et al. 1989; Colangeli et al. 1994; Koike et al. 1995; Mutschke et al. 1995, 2004; Reich 2011; Andersen et al. 1998; Braatz et al. 2000; Hill et al. 1998; Chen et al. 2002; Sheu et al. 2002; Jones et al. 2004; Pirali et al. 2007; Steglich et al. 2011; Usoltseva et al. 2018; Zhigilei et al. 1997a). The hope is that we can, at the very least, use these data to enable us to determine nano-diamond sizes in interstellar media through the ratio of the 3.43 μm and 3.53 μm band strengths (e.g. Chen et al. 2002; Sheu et al. 2002; Pirali et al. 2007) because, as these works show, this ratio is size dependent. However, the band ratio is also morphology-dependent (e.g. Pirali et al. 2007) and also depends on the nature and degree of the surface hydrogen coverage. Further, and given that nano-diamonds are observed in emission close to hot stars, this ratio will be temperature-dependent because of the underlying thermal continuum and the possibility of differential excitation and/or the de-hydrogenation of surface CH and CH₂ groups.

2.1. Possible degeneracies and critical assumptions

It is essential to understand and, where possible, to try and break the inherent degeneracies that must exist between the effects of particle size, shape, structure, composition, and degree of surface (de-)hydrogenation. In the latter case, we clearly need a detailed understanding of how (de-)hydrogenation may (dis)proportionately effect the CH/CH₂ surface concentration ratio, that is its effect on the relative contributions of CH_{*n*} groups at particles vertices, edges, and faces (e.g. Pirali et al. 2007).

The 3.43 μm and 3.53 μm band strengths and ratios have not yet been completely calibrated because the particle shapes in most infrared (IR) studies were not determined (e.g. Chen et al. 2002; Sheu et al. 2002). This was not the case for the small diamondoids ($N_C < 100$) studied by Pirali et al. (2007) where the particle shapes were principally tetrahedral and the 3.53/3.43 μm band ratio appears to be approximately linearly-dependent upon the CH/CH₂ surface concentration ratio.

However, it should be noted that a tetrahedral form for larger diamondoids or nano-diamonds may not be the most likely or even the most stable form in either a fully hydrogenated or a fully dehydrogenated state (e.g. Barnard et al. 2003a; Barnard & Zapol 2004).

In this work we, preliminarily at least, assume that the intrinsic 3.53 μm CH band peak intensity per CH group is ≈ 1.2 times that of the 3.43 μm CH₂ group, as indicated in the Pirali et al. (2007) simulations². This calibration, based on the smaller, tetrahedral diamondoids, may no longer hold true for different shapes and/or larger nano-diamonds. However, we have no choice but to ignore this possibility until such time as suitable laboratory data become available to refute this supposition.

2.2. Bulk density, number of C atoms, and surface coverage

Using the regular diamond lattice structure we can construct particles with a given number of C atoms as a model for interstellar nano-diamonds. The number of constituent C atoms in a particle can be determined from the particle volume, for example $(4/3)\pi abc$, for ellipsoids ($a \neq b \neq c$), spheroids ($a \neq b = c$), and spheres ($a = b = c$), and the bulk diamond specific density (here taken to be $\rho_{\text{bulk}} = 3.51 \text{ g cm}^{-3}$). Nevertheless, the density of a particle does exhibit some dependence on its size, as shown experimentally for 30–200 nm radius silica (SiO₂) nanoparticles, which have densities of $\sim 1.9 \text{ g cm}^{-3}$, which is 14–30% lower than that of the parental solid ($2.2\text{--}2.7 \text{ g cm}^{-3}$, Kimoto et al. 2014). Thus, and by analogy with silica, a structure not too dissimilar to that of diamond, and as in the THEMIS modelling (Jones et al. 2017), we should perhaps assume a diamond density reduction of the order of 20% for sub- μm particles. However, for the present purposes, given that the density must be depth-dependent and that we consider polyhedral shapes, we assume the bulk diamond density because our network modelling approach assumes a sp³ diamond C–C bond length of 0.154 nm and therefore a density of 3.51 g cm^{-3} .

In order to determine the number of C atoms in a particle, N_C , and because we are dealing with H atoms only at the surfaces, we assume that the mean atomic mass of the ‘bulk’ interior of a nano-diamond is that of a C atom, $A_C = 12 \text{ amu}$. The number of C atoms per particle is then given by

$$N_C = \frac{V_{\text{nd}}(S) \rho_{\text{bulk}}}{A_C m_H} \approx 734 \left(\frac{a}{1 \text{ nm}} \right)^3, \quad (1)$$

where $V_{\text{nd}}(S)$ is the nano-diamond shape-dependent volume and the right hand expression gives N_C for a spherical nano-diamond. Given that nitrogen is the most common diamond hetero-atom, the inclusion of a number of N atoms, N_N , within the bulk can be expressed as a fraction, f_N , of the total number of C atoms, that is $N_N = f_N \times N_C$. In this case the mean atomic mass of the ‘bulk’ would then need to be adjusted accordingly, that is $A_{C(N)} = (1 - f_N) \times A_C + f_N \times A_N$ where $A_N = 14$.

The fraction of C atoms that are at the particle surface depends upon the shape and will therefore be determined on a shape-by-shape basis. For (nano)diamond particles this depends upon the numbers of CH and CH₂ groups (per unit edge length or per unit surface area) on particle vertices, edges and faces.

For carbon atoms within the diamond bulk the C–C–C bond angle is 109.5°, the tetrahedral angle, the projected distance of the 0.154 nm C–C bond length (d_{C-C}) onto a

² The experimental results for the 3.53/3.43 μm band ratio in the polyamantanes in the Pirali et al. (2007) study are, however, less clear-cut.

{100} facet³ is 0.126 nm and the distance between CH₂ groups on this surface or along {111}–{111} and {111}–{100} edges is $(2 \times 0.126) = 0.252$ nm ($= D_{\text{CH}_2}$). The area per CH₂ group on a {100} facet is then $(2 \times 0.126)^2 \text{ nm}^2 = 0.0635 \text{ nm}^2$ because, viewed perpendicularly, the {100} surface appears as a 0.126 nm \times 0.126 nm square grid with one CH₂ group per four squares. Therefore, {100} facets present one CH₂ group per 0.0635 nm² ($= A_{\text{CH}_2}$), or one H atom per 0.0318 nm². In contrast, {111} facets present a hexagonal grid with projected C–C bond length sides of 0.126 nm, and area $(3/2)\sqrt{3} \times 0.126^2 \text{ nm}^2 = 0.0412 \text{ nm}^2$, with one CH bond per hexagon, and one CH group or one H atom per 0.0412 nm² ($= A_{\text{CH}}$). The H atom density on {100} facets is $\approx 30\%$ greater than on {111} facets but CH groups are $\approx 35\%$ more abundant on {111} facets.

In our calculations, we derived the shape-dependent group abundance ratio, $\{[\text{CH}]/[\text{CH}_2]\}_S$ ⁴, and the model-predicted IR band ratio is then

$$I(3.53 \mu\text{m})/I(3.43 \mu\text{m}) = R_{\text{IR}} \times \{[\text{CH}]/[\text{CH}_2]\}_S, \quad (2)$$

where R_{IR} is the measured ratio of the 3.53 μm and 3.43 μm band intensities, that is $I_{3.53}(\text{CH})/I_{3.43}(\text{CH}_2) \approx 1.2$ (e.g. Pirali et al. 2007)⁵. In the following we calculated and present the abundance ratio, $[\text{CH}]/[\text{CH}_2]$, leaving the user to adjust the required numbers by their preferred value for R_{IR} .

3. Shape and surfaces

The infrared bands observed to date in proto-planetary discs that are attributed to nano-diamond are, primarily, the 3.43 and 3.53 μm CH_{*n*} stretching bands, which are characteristic of diamond {100} and {111} surfaces or facets passivated by H atoms in CH₂ and CH groups, respectively. Given this facet-specificity we clearly must consider all of the possible and likely euhedral forms that nano-diamonds are known to exhibit in the laboratory along with their respective surface CH_{*n*} functionalisation.

From images of synthetic nano-diamonds and CVD diamond coatings it appears that a wide range of particle shapes is possible, including: truncated octahedral, cuboctahedral, tetrahedral, and cubic particles. For completeness we therefore consider all possible euhedral forms, from tetrahedral to cubic and all intervening polyhedra, including: regular tetrahedra, octahedra, and cubes and their regular and semi-regular truncated forms. For brevity in the following, we define the following designators for the various forms: T, tT, O, tO, cO, tC, and C, for tetrahedra, truncated tetrahedra, octahedra, truncated octahedra, cuboctahedra, truncated cubes, and cubes, respectively (see Fig. 1). The edges of regular particles are all of equal length, while semi-regular truncated polyhedra have truncated vertex facets of variable edge length, that is all of the edges bordering the triangular and square truncation faces are of the same length and can differ in length from the other edges. In truncated polyhedra the hexagonal and octagonal faces are transposed into six- and eight-sided faces with alternating edges of differing lengths. The regular polyhedral forms, with all edges of equal length, are shown in Fig. 1

³ A facet is a particular crystallographic plane, face or facet indicated by $\{h, k, l\}$ where $h, k,$ and l are the Miller indices, which are the minimised integer distances along the respective $x, y,$ and z crystalline axes.

⁴ For simplicity this ratio is hereafter written as $[\text{CH}]/[\text{CH}_2]$.

⁵ N.B., This is equivalent to a ratio of 0.6 when normalised to the number of hydrogen atoms involved.

along with their fundamental characteristics. In addition to these forms, we also considered ‘spherical’ nano-diamonds.

Based on the studies of Barnard & Sternberg (2005) and Pirali et al. (2007), but primarily following the modelling of regular and semi-regular polyhedra and their truncated forms presented here, we make the following observations: vertices are terminated with CH (T) or CH₂ (O) groups, the edges between {111} facets are CH₂ (T) or CH (O), all three- and six-sided faces are {111} facets, all four- and eight-sided faces are {100} facets, {111} facets exhibit only coherently-directed CH bonds and {100} facets are CH₂-covered. In the non-specified cases vertex CH_{*n*} structures form part of the adjacent edges and edge CH_{*n*} structures form part of the adjacent faces⁶. These results are summarised in Table 1.

For a given polyhedron the fractional surface area in triangular and/or hexagonal {111} facets is denoted as $f_{s\{111\}}$ and that in square and/or octagonal {100} facets as $f_{s\{100\}}$. The number of surface C and H atoms per particle, $N_{\text{Cs}\{111\}}, N_{\text{Hs}\{111\}}, N_{\text{Cs}\{100\}}$ and $N_{\text{Hs}\{100\}}$ in {111} and {100} facets respectively, are then:

$$N_{\text{Cs}\{111\}} = f_{s\{111\}} N_{\text{Cs}}, \quad N_{\text{Hs}\{111\}} = N_{\text{Cs}\{111\}} f_{\text{H}}, \quad (3)$$

and

$$N_{\text{Cs}\{100\}} = f_{s\{100\}} N_{\text{Cs}}, \quad N_{\text{Hs}\{100\}} = 2 N_{\text{Cs}\{100\}} f_{\text{H}}, \quad (4)$$

where f_{H} is the degree of surface hydrogenation, with $f_{\text{H}} = 1$ indicating a maximally-hydrogenated surface and $f_{\text{H}} = 0$ a completely dehydrogenated surface.

4. Regular polyhedral particles

Here, we consider the case of regular polyhedral particles, and their truncated variants, where all edges are of equal length, l . The full expressions for the properties and characteristics of regular polyhedral particles can be found in Appendix A. We recall that regular triangular and hexagonal {111} facets have areas of $\sqrt{3}/4 l^2$ and $3\sqrt{3}/2 l^2$, respectively, and that regular square and octagonal {100} facets have areas of l^2 and $2(\sqrt{2} + 1)l^2$, respectively⁷.

For all of the polyhedral nano-diamond particle shapes considered here the total number of CH groups is obtained by summing over their number on vertices (V_{CH}), edges (E_{CH}), and triangular and hexagonal {111} facets ($F_{\{111\}}(\Delta\circ)$) and the number of CH₂ groups by summing over those on vertices (V_{CH_2}), edges (E_{CH_2}), and square and octagonal {100} facets ($F_{\{100\}}(\square\circ)$). The $[\text{CH}]/[\text{CH}_2]$ ratio is then obtained via,

$$\frac{[\text{CH}]}{[\text{CH}_2]} = \frac{V_{\text{CH}} + E_{\text{CH}} + F_{\{111\}}(\Delta\circ)}{V_{\text{CH}_2} + E_{\text{CH}_2} + F_{\{100\}}(\square\circ)}. \quad (5)$$

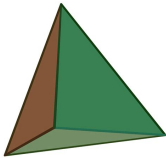
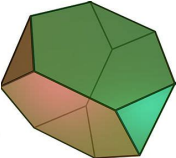
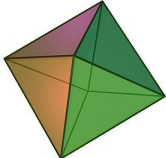
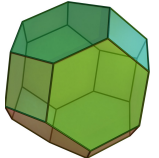
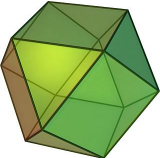
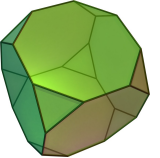
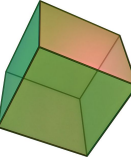
From the observations drawn at the end of the previous section, it follows that where vertices (edges) are of the same CH_{*n*} type as an adjacent edge (facet) then they are subsumed into that edge (facet).

To determine the various polyhedral behaviours the reader should make extensive reference to Fig. 1 and Tables 1 and 2 to derive the quantities $V_{\text{CH}_n}, E_{\text{CH}_n}, F_{\{111\}}$ and $F_{\{100\}}$, and this should be taken as implicit in the following subsections and is therefore

⁶ This is strictly only valid for infinitely small vertices and infinitely thin edges but is a good approximation for particle sizes $\gg d_{\text{C-C}}$.

⁷ In this and the following section we implicitly assumed that the polyhedral edge lengths, l , are in units of the C–C bond length $d_{\text{C-C}}$, even though they are not actually discretised in this way.

Regular polyhedra with equal length edges

tetrahedron	truncated tetrahedron	octahedron	truncated octahedron	cuboctahedron	truncated cube	cube
T	tT	O	tO	cO	tC	C
						
V = 4	12	6	24	12	24	8
E = 6	18	12	36	24	36	12
F = 4	8	8	14	14	14	6
$f_{s\{111\}} = 1$	1	1	0.776	0.366	0.107	0
$V/V_{\text{sph.}} = 0.123$	0.401	0.318	0.683	0.563	0.577	0.368

V, E and F are the number of vertices, edges and faces ($V - E + F = 2$, is the Euler characteristic).

In diamond triangular and hexagonal facets are $\{111\}$ and square and octagonal facets are $\{100\}$.

$V/V_{\text{sph.}}$, the 'sphericity', is the volume of the polyhedron/volume of the circumscribed sphere.

Fig. 1. Regular polyhedra and their truncated forms along with some of their properties. $f_{s\{111\}}$ is the fraction of the particle surface in triangular and hexagonal facets. We note that all square and octagonal facets are $\{100\}$.

Table 1. Polyhedral nano-diamond particle vertex (V), edge (E) and face (F) properties.

Shape	V	Vertices	E	Edges	F	Faces	$f_{s\{111\}}$	$r_{\text{eff}}/a_{\text{nd}}$
T	4	4 isolated CH	6	$6 \times \{111\}/\{111\}$, CH ₂	4	$4 \times \{111\}$ triangular, CH	1	2.013
tT	12	≡ edge CH ₂	18	$6 \times \{111\}/\{111\}$, CH ₂ $12 \times \{111\}/\{111\}$, CH on faces	8	$4 \times \{111\}$ hexagonal, CH $4 \times \{111\}$ triangular, CH	1	1.356
O	6	6 isolated CH ₂	12	$12 \times \{111\}/\{111\}$, CH on faces	8	$8 \times \{111\}$ triangular, CH	1	1.465
tO	24	≡ face CH	36	$24 \times \{111\}/\{100\}$, CH ₂ on faces $12 \times \{111\}/\{111\}$, CH on faces	14	$6 \times \{100\}$ square, CH ₂ $8 \times \{111\}$ hexagonal, CH	0.776	1.135
cO	12	≡ face CH ₂	24	$24 \times \{111\}/\{100\}$, CH ₂ on faces (all cO edges are equivalent)	14	$6 \times \{100\}$ square, CH ₂ $8 \times \{111\}$ triangular, CH	0.366	1.211
tC	24	≡ face CH ₂	36	$24 \times \{111\}/\{100\}$, CH ₂ on faces $12 \times \{100\}/\{100\}$, CH ₂ on faces	14	$6 \times \{100\}$ octagonal, CH ₂ $8 \times \{111\}$ triangular, CH	0.107	1.396
C	8	4 CH ₂ + 4 CH ₃	12	$12 \times \{100\}/\{100\}$, CH ₂ on faces	6	$6 \times \{100\}$ square, CH ₂	0	1.201

Notes. Only $\{111\}$ and $\{100\}$ facets are considered in the modelling where $f_{s\{111\}}$ is the fraction of the particle surface in $\{111\}$ facets and therefore $f_{s\{100\}} = (1 - f_{s\{111\}})$. The considered regular polyhedral shapes are tetrahedra (T), truncated tetrahedra (tT), octahedra (O), truncated octahedra (tO), cuboctahedra (cO), truncated cubes (tC), and cubes (C). For vertices '≡ edge(face) CH_n' indicates that their CH_n groups can be considered as forming an integral part of the adjacent edges (faces). The last column gives the ratio of the radius of the circumscribed sphere, r_{eff} , with the same volume as a sphere, a_{nd} (see text for details).

not be repeated at every instance. In Table 1 polyhedral vertices indicated as '≡ edge CH_n' or '≡ face CH_n' do not count as independent CH_n groups because they are of the same type as an adjacent edge or face and therefore already counted as a part of

that edge or face, which is to their right in the table. Similarly, edges labelled as 'on faces' are already counted as part of the adjacent face. This is generally manifest where horizontally adjacent V and E or E and F entries in the table have identical CH_n

Table 2. Nano-diamond polyhedra vertex (V), edge (E), and face (F) hierarchies as a function of CH_n group composition and facet geometry.

Shape	CH _n	V	E	F	[CH]/[CH ₂]
T	CH ₂	–	6	–	$\propto l$
	CH	4	–	4Δ	
tT	CH ₂	12→	6	–	$\propto l$
	CH	–	12→	4Δ4\circ	
O	CH ₂	6	–	–	$\propto l^2$
	CH	–	12→	8Δ	
tO	CH ₂	–	24→	6\square	$2\sqrt{3}$
	CH	24→	12→	8\circ	
cO	CH ₂	12→	24→	6\square	$\frac{1}{3}\sqrt{3}$
	CH	–	–	8Δ	
tC	CH ₂	24→	36→	6\circ	$\frac{\sqrt{3}}{6(\sqrt{2+1})}$
	CH	–	–	8Δ	
C	CH _{2,3}	8→	12→	6\square	0
	CH	–	–	–	

Notes. Rightward arrows indicate that a given quantity is subsumed into the quantity to its right, i.e. V→E, E→F or V→E→F and therefore that only the boldface quantities need to be included in order to avoid double counting. The [CH]/[CH₂] ratio behaviours are indicated in the right hand column.

group types. These dependencies are also shown more explicitly and concisely as arrows in Table 2. In the calculation of the polyhedral [CH]/[CH₂] ratios only the boldfaced quantities in Table 2 were included in order to avoid double counting CH_n groups.

The number of vertices for a given polyhedron is fixed, the total edge length scales with l and the facet area scales with l^2 . Thus, for large polyhedra, large with respect to the C–C bond length (i.e. $l \gg d_{C-C}$), it is the nature of the edges and facets that determine the [CH]/[CH₂] ratio and that in very large polyhedra ($l \gg d_{C-C}$) the size dependence of this ratio is principally driven by the l^2 dependence of the relevant facet areas.

4.1. Regular tetrahedral (T) particles

We first consider regular tetrahedral particles, the simplest regular polyhedra, with four CH vertices, $V_{CH} = 4$, six CH₂ edges, $E_{CH_2} = 6l$, and a total surface area of $F_{\{111\}(\Delta)} = 4 \times \sqrt{3}/4 l^2$. In this case, V_{CH_2} , E_{CH} and $F_{\{100\}}$ are all zero and so we have

$$\frac{[CH]}{[CH_2]} = \frac{V_{CH} + F_{\{111\}(\Delta)}}{E_{CH_2}} = \frac{4 + \sqrt{3} l^2}{6l}, \quad (6)$$

which reduces to $\approx(\sqrt{3}/6)l$ for large l . Thus, for regular tetrahedral nano-diamonds [CH]/[CH₂] increases with particle size as shown in Fig. 2.

4.2. Regular truncated tetrahedral (tT) particles

Regular truncated tetrahedral particles are tetrahedra with the four vertices truncated into equilateral triangular faces. They have 12 CH₂ vertices counted within the CH₂ edges, and therefore $V_{CH_2} = 0$, eighteen edges of which the 12 CH edges are counted within the adjacent {111} facets, yielding

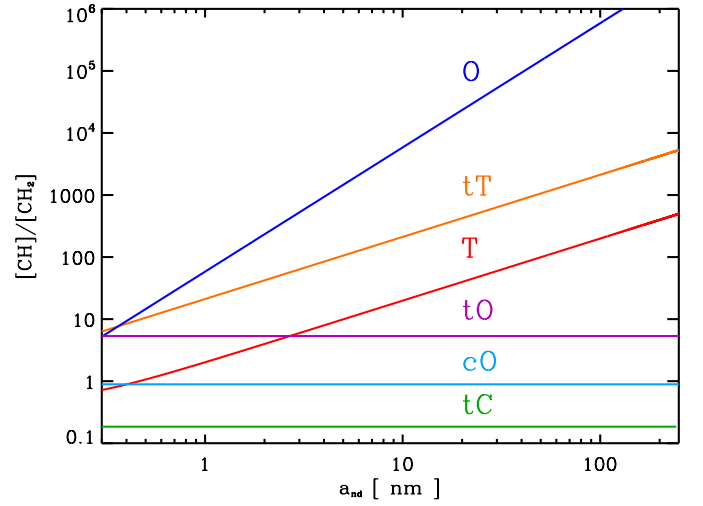


Fig. 2. [CH]/[CH₂] ratios for regular polyhedra as a function of the effective nano-diamond radius, a_{nd} (nm), for T (red), tT (orange), O (blue), tO (purple), cO (cobalt), and tC (green) forms. For the cubic form (C) this ratio is zero.

$E_{CH} = 0$ and $E_{CH_2} = 6l$, and a surface comprised of four triangular {111} facets and four hexagonal {111} facets. Thus, $F_{\{111\}(\Delta\circ)} = 4 \times \sqrt{3}/4 l^2 + 4 \times 3\sqrt{3}/2 l^2 = 7\sqrt{3} l^2$, and with V_{CH} and $F_{\{100\}}$ equal to zero, we have

$$\frac{[CH]}{[CH_2]} = \frac{F_{\{111\}(\Delta\circ)}}{E_{CH_2}} = \frac{7\sqrt{3}}{6} l. \quad (7)$$

Thus, as indicated in Fig. 2, the [CH]/[CH₂] ratio for regular truncated tetrahedral nano-diamonds increases with l (increasing size) and with the same slope as for T particles.

4.3. Regular octahedral (O) particles

Turning to regular octahedral particles with six CH₂ vertices, $V_{CH_2} = 6$, 12 CH edges all of which are counted within the adjacent {111} facets ($\therefore E_{CH} = 0$) and eight triangular {111} facets, $F_{\{111\}(\Delta)} = 8 \times \sqrt{3}/4 l^2 = 2\sqrt{3} l^2$. With V_{CH} , E_{CH_2} , and $F_{\{100\}}$ all zero, we have

$$\frac{[CH]}{[CH_2]} = \frac{F_{\{111\}(\Delta)}}{V_{CH_2}} = \frac{\sqrt{3}}{3} l^2. \quad (8)$$

As for tetrahedral nano-diamond polyhedra, the [CH]/[CH₂] ratio increases with size but in this case with a steeper l^2 dependence (Fig. 2).

4.4. Regular truncated octahedral (tO) particles

A common nano-diamond particle shape is the regular truncated octahedron (e.g. Barnard & Sternberg 2005), an octahedron with its six vertices truncated into square {100} facets. This polyhedron has 24 CH vertices and 36 edges (24 CH₂ and 12 CH) all of which can be counted within the adjacent edges and facets, respectively ($\therefore V_{CH}$, V_{CH_2} , E_{CH} , E_{CH_2} are all zero). The surface is comprised of eight hexagonal {111} facets and six square {100} facets, that is $F_{\{111\}(\circ)} = 8 \times 3\sqrt{3}/2 l^2 = 12\sqrt{3} l^2$ and $F_{\{100\}(\square)} = 6 l^2$, and

$$\frac{[CH]}{[CH_2]} = \frac{F_{\{111\}(\circ)}}{F_{\{100\}(\square)}} = 2\sqrt{3}, \quad (9)$$

for regular truncated octahedral nano-diamonds the [CH]/[CH₂] ratio is therefore independent of size (Fig. 2), in contrast to all of the previously considered polyhedral forms.

4.5. Regular cuboctahedral (cO) particles

Nano-diamonds also commonly form cuboctahedra, which are a limiting form of tO particles where the hexagonal faces are reduced to triangular faces. These interesting polyhedra have 12 CH₂ vertices and 24 CH₂ edges, all of which can be counted within the adjacent square {100} facets (i.e. V_{CH₂} and E_{CH₂} = 0). Their surfaces exhibit eight triangular {111} facets and six square {100} facets, F_{{111}(Δ)} = 8 × √3/4 l² = 2√3 l², F_{{100}(□)} = 6 l², and with V_{CH} and E_{CH} each zero, we have

$$\frac{[\text{CH}]}{[\text{CH}_2]} = \frac{F_{\{111\}(\Delta)}}{F_{\{100\}(\square)}} = \frac{\sqrt{3}}{3}, \quad (10)$$

and for this common nano-diamond polyhedral shape the [CH]/[CH₂] ratio is also independent of size, as per the closely related truncated octahedral polyhedron (Fig. 2).

4.6. Regular truncated cube (tC) particles

For completeness we finally consider the regular truncated cube, a cube with its eight vertices truncated into triangular facets. This polyhedron has 24 CH₂ vertices and 36 CH₂ edges, all of which can be counted within the adjacent octagonal {100} facets (i.e. V_{CH₂} and E_{CH₂} = 0). Their surfaces consist of eight triangular {111} facets and six octagonal {100} facets, F_{{111}(Δ)} = 8 × √3/4 l² = 2√3 l², F_{{100}(○)} = 6 × 2(√2 + 1) l² = 12(√2 + 1) l², and with V_{CH} and E_{CH} both zero, we have

$$\frac{[\text{CH}]}{[\text{CH}_2]} = \frac{F_{\{111\}(\Delta)}}{F_{\{100\}(\circ)}} = \frac{\sqrt{3}}{6(\sqrt{2} + 1)}, \quad (11)$$

and for truncated cubic nano-diamonds the [CH]/[CH₂] ratio is also independent of size, as per tO and cO polyhedral particles (Fig. 2).

4.7. Regular cube (C) particles

Another typical diamond shape is the regular cube, with 8 vertices, four of which are CH₂ and four CH₃, 12 CH₂ edges and 6 CH₂ facets, that is

$$\frac{[\text{CH}]}{[\text{CH}_2]} = \frac{0}{V_{\text{CH}_3} + V_{\text{CH}_2} + E_{\text{CH}_2} + F_{\{100\}(\square)}}. \quad (12)$$

Thus, given that there are no CH groups on perfectly cubic nano-diamonds their [CH]/[CH₂] ratios are zero.

4.8. The spatial properties of regular polyhedra

In the preceding sub-sections, we briefly derived the expected [CH]/[CH₂] ratios for regular polyhedral nano-diamonds. The results are graphically summarised in Fig. 2 where the ratio is plotted as a function of the effective radius a_{nd} for T (red), tT (orange), O (blue), tO (purple), cO (cobalt), and tC (green) particle forms (see Appendix A for the derivation of the effective nano-diamond radii, a_{nd}). In Fig. 2 we take into account the discrete nature of nano-diamonds and calculate the [CH] and [CH₂] surface abundances using the parameters D_{CH_2} , A_{CH_2} , and A_{CH} defined in Sect. 2.2. This figure indicates that [CH]/[CH₂] for

the closely related tO, cO, and tC polyhedra⁸ are independent of particle size. However, for the T, tT, and O polyhedra the [CH]/[CH₂] ratio, and hence the 3.53 μm(CH)/3.43 μm(CH₂) IR band ratio, does depend on size, and more strongly so for O than the T and tT polyhedra, and can span orders of magnitude.

The primary motivation for this study was to better understand the 3.53 μm(CH)/3.43 μm(CH₂) IR band intensity ratio, through a study of the surface [CH]/[CH₂] abundance ratio on nano-diamond {111} and {100} facets. It is therefore interesting to note the wide variation in the CH-covered, {111} facet surface fraction, $f_{s\{111\}}$, which while not strongly dependent on polyhedral form, is independent of size and spans about an order of magnitude (0.107–1.000, see Fig. 1).

We conclude that, if the observed nano-diamond shapes are polyhedral, but the distribution of polyhedral forms is not well determined, deriving the intrinsic [CH]/[CH₂] ratio can be uncertain by orders of magnitude. However, if the [CH]/[CH₂] ratio and size are known then it would be possible to usefully constrain the form or, conversely, to constrain the size if the [CH]/[CH₂] ratio and form are known. Ideally, and in order to maximise the amount of information from nano-diamond IR spectra, we therefore need to know the particle size and shape distributions. Unfortunately, astronomical observations cannot access either of these critical quantities and it is therefore going to be difficult to lift this degeneracy other than through detailed nano-particle modelling. Additionally, current presolar nano-diamond studies, while constraining particle sizes, do not provide sufficient information on the particle shapes⁹.

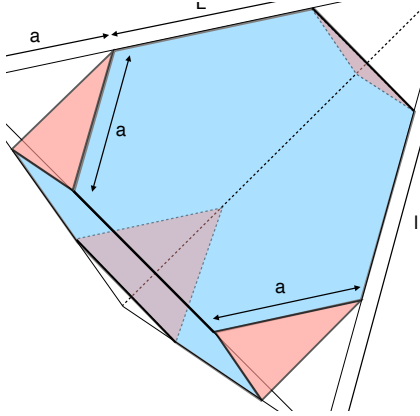
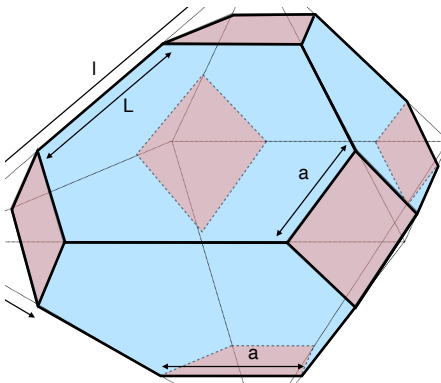
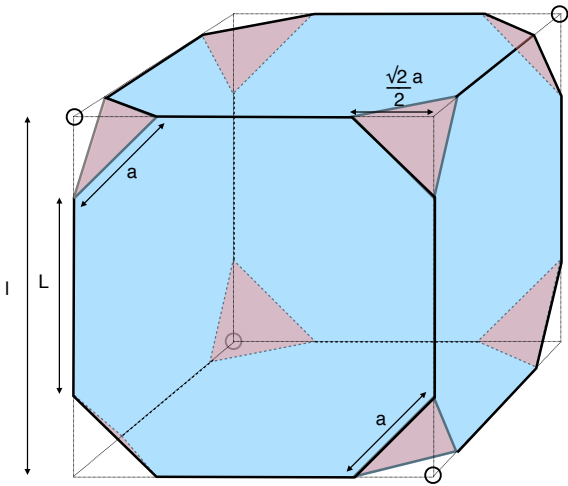
In this modelling scheme the forms are contiguous, meaning that the polyhedral dimensions can be scaled arbitrarily, that is the equations of these structures are not discretised. However, the numerical results presented in Fig. 2 do assume the appropriate C–C bond length, $d_{\text{C–C}}$, and CH_{*n*} group areas, A_{CH} , and A_{CH_2} . A more detailed treatment of the polyhedral particle geometries can be found in Appendices A and B. In our later diamond-bonded network modelling (Sect. 6) all of the calculations are necessarily discretised.

5. Semi-regular polyhedral particles

Wishing to generalise the method, but probably also complicate matters a little further, we now turn our attention to semi-regularly truncated polyhedra, which are semi-regular in the sense that, with respect to the regular parent polyhedron (i.e. tetrahedron, octahedron, and cube), the truncated facets are of arbitrary size but remain parallel to those of the regular truncated form of the parent polyhedron. The necessarily more cumbersome expressions are available in full in Appendix B for the more courageous of readers. While the truncated facets remain parallel to those of the parent polyhedron their edges are of arbitrary length a , which implies that the remnant edge, L , of the regular polyhedron parent is reduced from l to $(l - 2a)$ as illustrated in Figs. 3 to 5, that is $L = (l - 2a)$. In semi-regular polyhedra the triangular and square faces retain their regular form, that is all edges are of the length a , and therefore have areas of $\sqrt{3}/4 a^2$ and a^2 , respectively. However, the hexagonal and octagonal faces

⁸ N.B., tO, cO, and tC polyhedra are transformable tO ↔ cO ↔ tC through variations in the relative area of the square faces, which become octagonal in the cO ↔ tC transition.

⁹ For even this scant information to be of use we would have to assume that there is an as yet unsubstantiated direct relationship between the presolar nano-diamonds and those responsible for the observed circumstellar 3.53 μm(CH) and 3.43 μm(CH₂) IR bands.


Fig. 3. Semi-regular truncated tetrahedron.

Fig. 4. Semi-regular truncated octahedron.

Fig. 5. Semi-regular truncated cube.

are no longer regular but have alternating edge lengths of a and L . The area of the six-sided faces is now $\sqrt{3}/4(l^2 - 3a^2)$, which gives the area of a regular hexagon area when $l = 3a$, and the area of the eight-sided faces is now $(l^2 - a^2)$, which corresponds to a regular octagon when $l = (\sqrt{2} + 1)a$. Although the expressions for these polyhedra cannot be reduced to simple functions of r , the radius of the sphere that circumscribes the particle and includes all its vertices, the particles can still be circumscribed by a sphere that encompasses all vertices.

The mathematical expressions for the semi-regular truncated polyhedra (stT, stO and stC) given in this section (see also

Appendix B) are valid for $0 \leq a \leq l/2$, that is the parent polyhedron edge is, at most, bisectable, which leads to the following critical conditions:

- i) $a = 0 \equiv L = l \rightarrow$ a regular parent polyhedron,
- ii) $a = l/3 \equiv L = a \rightarrow$ a regular truncated parent polyhedron,
- iii) $a = l/2 \equiv L = 0 \rightarrow$ a different polyhedron.

In the $a = l/2$ case the truncated tetrahedron solution is an octahedron, and for the truncated octahedron and truncated cube the solution is a cuboctahedron¹⁰.

For each semi-regular polyhedron type, and in the same way as for the regular polyhedra of Sect. 4, we can derive the [CH]/[CH₂] ratios using the same expressions but substitute the new edge length expressions and the modified surface areas for the six and eight sided facets. In this case the number and type of vertices are unchanged.

5.1. Semi-regular truncated tetrahedral (stT) particles

These are similar to truncated tetrahedral particles except that the four vertices are now arbitrarily truncated into equal equilateral triangular faces of edge length a (see Fig. 3). The total edge length is now $12a + 6(l - 2a) = 6l$, that is truncation does not change the total edge length compared to the parent tetrahedron¹¹. The [CH]/[CH₂] ratio for a generalised truncated tetrahedron is then

$$\frac{[\text{CH}]}{[\text{CH}_2]} = \frac{F_{\{111\}}(\Delta\circ)}{E_{\text{CH}_2}} = \frac{\sqrt{3}a^2 + \sqrt{3}(l^2 - 3a^2)}{6l} = \frac{\sqrt{3}[(l/a)^2 - 2]}{6(l/a^2)}. \quad (13)$$

This reduces to that for a regular tetrahedron, $(\sqrt{3}/6)l$, when $a = 0$, if we ignore the change in vertex CH_n composition. From this equation the behaviour of the [CH]/[CH₂] ratio is less obvious because of the dependency on both l and a but as Fig. 6 shows an increase in the truncation length leads to an increase in the ratio.

5.2. Semi-regular truncated octahedral (stO) particles

These are octahedral particles with the six vertices arbitrarily truncated into equal area square faces of edge length a . The total edge length is now $24a + 12(l - 2a) = 12l$, that is truncation does not change the total edge length with respect to the parent octahedron¹² (see Fig. 4). The surface is comprised of eight six sided $\{111\}$ facets and six square $\{100\}$ facets that is $F_{\{111\}}(\circ) = 8 \times \sqrt{3}/4(l^2 - 3a^2) = 2\sqrt{3}(l^2 - 3a^2)$ and $F_{\{100\}}(\square) = 6a^2$, and

$$\frac{[\text{CH}]}{[\text{CH}_2]} = \frac{F_{\{111\}}(\circ)}{F_{\{100\}}(\square)} = \frac{2\sqrt{3}(l^2 - 3a^2)}{6a^2} = \frac{\sqrt{3}}{3} \left[\left(\frac{l}{a}\right)^2 - 3 \right]. \quad (14)$$

This expression reduces to that for a regular truncated octahedron on substituting $l = 3a$ and to a regular cuboctahedron for $l = 2a$. Figure 6 shows that for semi-regular truncated octahedral nano-diamonds the [CH]/[CH₂] ratio increases with the increasing number of carbon atoms but decreases and tends to flatten with increasing truncation (increasing a). The latter effect is because the particle shapes are increasingly driven towards the tO and cO forms which exhibit size independent [CH]/[CH₂] ratios.

¹⁰ Hence, cO particles are not considered here because they are the stO and stC polyhedra formed by bisecting the parent polyhedron edges.

¹¹ This is because the chamfered vertices are regular tetrahedra.

¹² In this case the chamfered vertices are half of a regular octahedron.

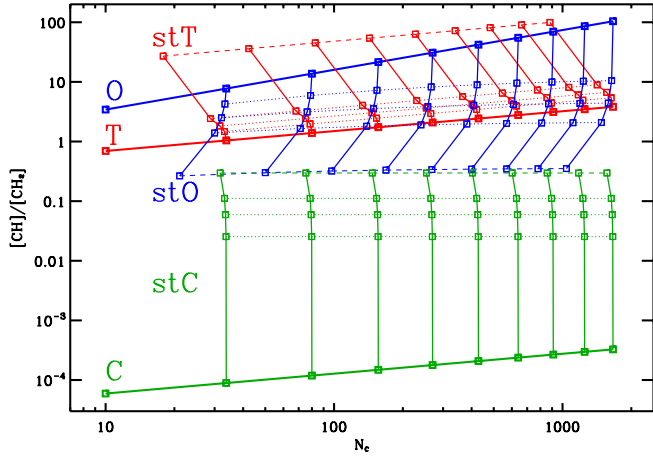


Fig. 6. $[\text{CH}]/[\text{CH}_2]$ ratios in semi-regular truncated polyhedra, stT (red), stO (blue), and stC (green), as a function of the truncation length ($a=0$ [thick], $\frac{1}{6}l$, $\frac{1}{4}l$, $\frac{1}{3}l$ [dotted], $\frac{1}{2}l$ [dashed]), and the number of constituent carbon atoms N_C . The thick lines show the data for the un-truncated polyhedra and the thin dashed lines show the $a=1/2$ limiting cases, except for stT where $a=0.49l$. The dangling and rising thinner lines show the effects of increasing truncation. For the C polyhedra, and for illustrative purposes only, an arbitrarily low value ($10^4 l$) of the $[\text{CH}]/[\text{CH}_2]$ ratio was assumed.

5.3. Semi-regular truncated cubic (stC) particles

These are cubes with the eight vertices arbitrarily truncated into equilateral triangular faces of edge length a . The total edge length is now $24a + 12[l - \sqrt{2}a] = [12l + 12a(2 - \sqrt{2})]$ (see Fig. 5) and therefore differs from that of the parent polyhedron in this case. The polyhedral surfaces consist of eight triangular $\{111\}$ facets and six eight-sided $\{100\}$ facets), $F_{\{111\}}(\Delta) = 8 \times \sqrt{3}/4 a^2 = 2\sqrt{3} a^2$, $F_{\{100\}}(\bigcirc) = 6 \times (l^2 - a^2)$ and

$$\frac{[\text{CH}]}{[\text{CH}_2]} = \frac{F_{\{111\}}(\Delta)}{F_{\{100\}}(\bigcirc)} = \frac{\sqrt{3} a^2}{6(l^2 - a^2)} = \frac{\sqrt{3}}{6 \left[(l/a)^2 - 1 \right]}. \quad (15)$$

In the case of truncated cubic nano-diamonds the $[\text{CH}]/[\text{CH}_2]$ ratios launch from zero because cubic particle surfaces are comprised of only CH_2 groups. Thereafter their $[\text{CH}]/[\text{CH}_2]$ behaviour is determined by the denominator in the above expression. Thus, with increasing truncation (l/a) decreases and the $[\text{CH}]/[\text{CH}_2]$ ratio increases steeply, and much more so than the increase for stT and the decrease for stO polyhedra, as can be clearly seen in Fig. 6. It is interesting to note the convergence of the stC and stO polyhedra in this figure, which is due to the fact that both of these forms converge to the related cO polyhedral form with increasing truncation.

5.4. The spatial properties of semi-regular polyhedra

Figure 6 shows the $[\text{CH}]/[\text{CH}_2]$ ratios of semi-regular truncated polyhedra, stT (red), stO (blue), and stC (green), as a function the number of constituent carbon atoms N_C . Most of what we noted in Sect. 4.8, pertaining to the $[\text{CH}]/[\text{CH}_2]$ ratio in regular polyhedra, also holds for semi-regular polyhedra and so it will not be repeated here.

We note that the truncation of tetrahedral (T) and octahedral (O) particles, to tT and tO, respectively, leads to an overlap in their $[\text{CH}]/[\text{CH}_2]$ ratios and that truncated cubic particles (stC) always have lower ratios because of the dominance of $\{100\}$ facets. The limiting stC particles converge with the limiting stO

forms because, at maximum truncation, the stO and stC forms both converge to cO polyhedra.

It is evident that the truncation of tetrahedral polyhedra can sequentially result in tT, O, tO, and cO forms, and with square $\{100\}$ facet expansion, to tC and C polyhedra, and that is there is therefore a two-way transformational sequence

$$\text{T}_{0.12}^4 \leftrightarrow \text{tT}_{0.40}^8 \leftrightarrow \text{O}_{0.32}^8 \leftrightarrow \text{tO}_{0.68}^{14} \leftrightarrow \text{cO}_{0.56}^{14} \leftrightarrow \text{tC}_{0.58}^{14} \leftrightarrow \text{C}_{0.37}^6$$

where the subscript is the ‘sphericity’ (to 2 d.p.) and the superscript is the number of faces (F) in the given polyhedron. The above sequence, which was alluded to at the beginning of Sect. 5, implies that some of the ‘upward’ tetrahedral truncation evolution in Fig. 6 must lead to some exact regular polyhedral solutions. However, the counter ‘downward’ octahedral truncation in this figure does not represent a reversal of the above transformation, even though there is an overlap in the mapped-out parameter space. This is because there is, in general, likely to be an increase in the ‘sphericity’ during any evolutionary sequence due to erosion, that is there will be a ‘blunting’ of the protruding polyhedral vertices and exposed edges. This can be seen along the transformation sequence shown above as a general correlation between ‘sphericity’ and the number of faces (F). However, cubic polyhedra, although they may appear to be a bit of an outlier to this trend, are nevertheless a part of this sequence, which is in fact a cycle. This is because a $\text{C} \leftrightarrow \text{T}$ polyhedral transformation is possible via the half-truncated cube, that is a cube in which only the opposing vertices on opposing faces (indicated by the small circles in Fig. 5) are chamfered into equilateral triangles.

Interestingly, the truncation of tetrahedra ($\text{T} \rightarrow \text{tT}$) and octahedra ($\text{O} \rightarrow \text{tO}$) initially leads to a convergence of their $[\text{CH}]/[\text{CH}_2]$ ratios, that is they evolve in opposite senses, and then to an overshoot of one another to more extreme values. Also evident in Fig. 6 is a progressive flattening of this ratio as octahedral particles are progressively truncated ($\text{O} \rightarrow \text{tO} \rightarrow \text{cO}$), which is to be expected because, as Fig. 2 indicates, the $[\text{CH}]/[\text{CH}_2]$ ratio in tO and cO particles is independent of size.

The results in Fig. 6 confirm the earlier conclusion that the nano-diamond $[\text{CH}]/[\text{CH}_2]$ ratio likely varies over more than an order of magnitude for any given size particle. As in the previous sections, the modelling of semi-regular polyhedra is a process in which the possible particle dimensions are continuous, that is any arbitrary polyhedral dimension is valid.

6. Diamond-bonded nano-particle networks

This section presents a diamond network bonding model, a complementary, discretised approach that is more attuned to the calculation of the ‘molecular’ structure of diamond at nano-scales, which can be directly compared with the (semi-)regular polyhedral models developed in the previous sections. The diamond lattice consists of two interwoven, face-centred cubic (fcc) lattices that are offset by one quarter of the unit cell dimension with respect to each other¹³. This overlapping two-fcc lattice deconstruction allows for a reasonably straight-forward, cubic-grid computational description of the perfect diamond lattice.

In this approach we consider the from-vertex ‘top-down’ atomic layers, i , of regular tetrahedral and octahedral structures (where $i = 1, 2, 3, 4, \dots$). Construction, or rather de-construction, is such that the removal of a particular atomic layer, and of

¹³ The lattice offset is one quarter of the unit cell dimension in each of the \hat{x} , \hat{y} , and \hat{z} directions, which are orthogonal in the diamond lattice.

its associated overlying atomic layers, leaves a coherent diamond(oid) particle with no ‘dangling’ CH_{*n*} groups (where *n* can be 1,2 or 3) and with the ‘newly-exposed’ surface passivated with only CH and CH₂ groups. In the following, and for simplicity, we designate the considered T, tT, O, and tO particles as diamondoids, even though they may not strictly be such. As a guide, and before we enter into the details in the following subsections, we present some general characteristics of this atomic layer approach.

For tetrahedral particles the sequential number of carbon atoms per layer, *n*, is given by the series of the squares:

$$n = 4, 9, 16, 25, 36, 49, 64, 81, 100, \dots$$

and for the *i*th atomic layer $N_C = (i + 1)^2$. Summing over this series does not yield the total number of carbon atoms in the particle because the terminating, lowest layer (largest value of *i*) has three less atoms than the series predicts¹⁴. Hence,

$$N_C = \left\{ \sum_i (i + 1)^2 \right\} - 3.$$

With this formalism the minimum tetrahedral particle, adamantane (C₁₀H₁₆), has the layer structure 4, (9 – 3) = 4, 6 and a total number of carbon atoms $N_C = (4 + 9) - 3 = 10$.

For octahedral particles the series for the number of carbon atoms per layer is:

$$n = 1, 2, 4, 6, 9, 12, 16, 20, 25, 30, 36, \dots$$

where this series effectively comprises alternating terms in the series with terms j^2 and $k(k + 1)$, respectively. Reflection about a square term $\geq 2^2$ (i.e. 4, 9, 16, 25, 36, ...) yields a complete octahedral nano-diamond particle. The minimum octahedral particle is also adamantane and in this formalism has the layer structure 1, 2, 4, 2, 1 ($N_C = 10$). For a 9-atomic layer octahedron the number of carbon atoms per layer is obtained by reflection about the $i = 5$ term ($j = 3 \equiv (i - 2)^2 = 3^2$) in the alternating series, i.e.

$$n = 1, 2, 4, 6, 9, 6, 4, 2, 1 \quad \sum_n = N_C = 35.$$

In the following we explore these two network structures in more detail in order to calculate their compositions and, in particular, their [CH]/[CH₂] group ratios.

6.1. Tetrahedral and truncated tetrahedral networks

The faces, edges and vertices of tetrahedral diamondoids are comprised of CH, CH₂, and CH groups, respectively. In their truncated forms the four CH-terminated vertices are replaced with four {111} CH-passivated facets and the {111}/{111} truncation edges are alternately-directed CH bonds coherent with the adjacent {111} facets.

With a bit of three-dimensional geometrical thinking it can be shown that the total number of carbon atoms, N_C , in a diamondoid with *i* atomic layers is given by

$$N_C = 6(2i - 1) + 4(i - 1)^2 + 4 + \left\{ \sum_i (i - 2)^2 \right\}, \quad (16)$$

where the terms are, from left to right, the number of edge, face, vertex, and quaternary (4°) carbon atoms. Replacing the summation with the closed formula $(i - 2)^3/3 + (i - 2)^2/2 + (i - 2)/6$ it can be shown that Eq. (16) reduces to

$$N_C = \frac{i^3}{3} + \frac{5i^2}{2} + \frac{37i}{6} + 1. \quad (17)$$

¹⁴ If allowed, these C atoms would form dangling CH₃ groups.

The corresponding number of hydrogen atoms is

$$N_H = 12i + 4 \frac{i(i - 1)}{2} + 4, \quad (18)$$

where the terms are, from left to right, the number of edge CH₂’s, and facet and vertex CH groups, respectively, which reduces to

$$N_H = 2i^2 + 10i + 4. \quad (19)$$

Truncation leads to the cumulative loss of successive layers, *i*, of carbon atoms, from each of the four vertices for equi-vertex truncation, following the atomic layers series described above, that is 16, 36, 64, 100, 144, 196, 256, ... $4(i + 1)^2$, which highlights the increasingly rapid loss of atoms with top-down truncation in a tetrahedral pyramid. The total number of carbon atoms lost, where all four vertices are equally truncated, is given by

$$N_{C,\text{loss}} = 4 \sum_i (i + 1)^2 = \frac{2i(2i^2 + 9i + 13)}{3}. \quad (20)$$

The equivalent hydrogen atom loss from all four vertices is

$$N_{H,\text{loss}} = 4 \left\{ 6i + 3 \sum_i (i - 1) - \sum_i (i + 1) \right\} = i(i + 3), \quad (21)$$

where the terms in brackets, from left to right, relate to the loss of CH₂, and the loss and gain of CH groups, respectively, that is

$$N_{\text{CH}_2,\text{loss}} = 12i \quad (22)$$

$$N_{\text{CH}_2,\text{gain}} = 0 \quad (23)$$

$$N_{\text{CH},\text{loss}} = 6i(i - 1) + 4 \quad (24)$$

$$N_{\text{CH},\text{gain}} = 2(i + 1)(i + 2). \quad (25)$$

The factor of two difference between the first term in Eqs. (21) and (22) is because the former counts the total H atom loss from CH₂ groups and the latter the number of CH₂ groups lost. The tetrahedral and truncated tetrahedral particle compositions are shown in Tables 3 and 4, respectively.

6.2. Octahedral and truncated octahedral networks

The faces, edges and vertices of octahedral diamondoids are comprised of CH, alternately-directed CH and CH₂ groups, respectively. In the truncated form the {100} truncation facets are CH₂ covered and the {100}/{111} truncation edges and vertices comprise CH bonds coherent with the adjacent {111} facets.

With yet another bout of three dimensional gymnastics it is possible to show that the total number of carbon atoms in a diamondoid with (2*i* + 1) atomic layers is given by

$$N_C = 2 \sum_i i^2 + 2 \sum_i i(i + 1)^2 + (i + 1)^2, \quad (26)$$

where the first two terms on the left give the number of mid-plane to vertex atoms and the right hand term is the number of atoms in the square mid-plane. Replacing the summations with their closed forms this reduces to

$$N_C = \frac{4i^3}{3} + 4i^2 + \frac{11i}{3} + 1. \quad (27)$$

Table 3. Tetrahedral particle compositions.

i	N_C	N_H	N_{CH}	N_{CH_2}	N_{4°	H/C	X_H	[CH]/[CH ₂]
1	10	16	4	6	0	1.60	0.62	0.67
2	26	32	8	12	6	1.23	0.55	0.67
3	51	52	16	18	17	1.02	0.50	0.89
4	87	76	28	24	35	0.87	0.47	1.17
5	136	104	44	30	62	0.76	0.43	1.47
6	200	136	64	36	100	0.68	0.40	1.78
7	281	172	88	42	151	0.61	0.38	2.10
8	381	212	116	48	217	0.56	0.36	2.42
9	502	256	148	54	300	0.51	0.34	2.74
10	646	304	184	60	402	0.47	0.32	3.07
11	814	356	224	66	524	0.44	0.30	3.39
12	1011	412	268	72	671	0.41	0.29	3.72

Notes. As a function of the number of atomic layers, i . N_C and N_H are the total number of carbon and hydrogen atoms, N_{CH} and N_{CH_2} the number of CH _{n} groups on the surfaces, N_{4° the number of carbon atoms in the bulk and X_H the atomic hydrogen fraction.

Table 4. Truncated tetrahedral particle compositions.

i	N_C	N_H	n	$N_C(n)$	$N_H(n)$	N_{CH}	N_{CH_2}	N_{4°	H/C	X_H	[CH]/[CH ₂]
3	51	52	1	35	36	24	6	5	1.03	0.51	4.00
4	87	76	1	71	60	36	12	23	0.85	0.46	3.00
5	136	104	1	120	88	52	18	50	0.73	0.42	2.89
			2	84	64	52	6	26	0.76	0.43	8.67
6	200	136	1	184	120	72	24	88	0.65	0.39	3.00
			2	148	96	72	12	64	0.65	0.39	6.00
7	281	172	1	265	156	96	30	139	0.59	0.37	3.20
			2	229	132	96	18	115	0.58	0.37	5.33
			3	165	100	88	6	71	0.61	0.38	14.67
8	381	212	1	365	196	124	36	205	0.54	0.35	3.44
			2	329	172	124	24	181	0.52	0.34	5.17
			3	265	140	116	12	137	0.53	0.35	9.67
9	502	256	1	486	240	156	42	288	0.49	0.33	3.71
			2	450	216	156	30	264	0.48	0.32	5.20
			3	386	184	148	18	220	0.48	0.32	8.22
			4	286	144	132	6	148	0.50	0.33	22.00
10	646	304	1	630	288	192	48	390	0.46	0.31	4.00
			2	594	264	192	36	366	0.44	0.31	5.33
			3	530	232	184	24	322	0.44	0.30	7.67
			4	430	192	168	12	250	0.45	0.31	14.00
11	814	356	1	798	340	232	54	512	0.43	0.30	4.30
			2	762	316	232	42	488	0.41	0.29	5.52
			3	698	284	224	30	444	0.41	0.29	7.47
			4	598	244	208	18	372	0.41	0.29	11.56
			5	454	196	184	6	264	0.43	0.30	30.67
12	1011	412	1	995	396	276	60	659	0.40	0.28	4.60
			2	959	372	276	48	635	0.39	0.28	5.75
			3	895	340	268	36	591	0.38	0.28	7.44
			4	795	300	252	24	519	0.38	0.27	10.50
			5	651	252	228	12	411	0.39	0.28	19.00

Notes. As a function of the number of atomic layers, i , and the number of atomic layer truncations, n . N_C and N_H are the total number of carbon and hydrogen atoms in the parent tetrahedron and $N_C(n)$ and $N_H(n)$ those in the truncated tetrahedron. N_{CH} and N_{CH_2} the number of CH _{n} groups on the surfaces, N_{4° the number of carbon atoms in the bulk and X_H the atomic hydrogen fraction.

Table 5. Octahedral particle compositions.

i	N_C	N_H	N_{CH}	N_{CH_2}	N_{4°	H/C	X_H	[CH]/[CH ₂]
0	10	16	4	6	0	1.60	0.62	0.67
1	35	36	24	6	5	1.03	0.51	4.00
2	84	64	52	6	26	0.76	0.43	8.67
3	165	100	88	6	71	0.61	0.38	14.67
4	286	144	132	6	148	0.50	0.33	22.00
5	455	196	184	6	265	0.43	0.30	30.67
6	680	256	244	6	430	0.38	0.27	40.67
7	969	324	312	6	651	0.33	0.25	52.00
8	1330	400	388	6	936	0.30	0.23	64.67

Notes. As a function of the number of atomic layers, i , N_C , and N_H are the total number of carbon and hydrogen atoms, N_{CH} and N_{CH_2} the number of CH _{n} groups on the surfaces, N_{4° the number of carbon atoms in the bulk and X_H the atomic hydrogen fraction.

The corresponding total number of hydrogen atoms is

$$N_H = (i + 3)^2. \quad (28)$$

The number of vertex CH₂ groups, N_{CH_2} , is constant at 6 (i.e. $N_{H,vertex} = 12$) and the number of CH groups in {111} facets and along their edges is then $N_{CH} = N_H - 12$.

Truncation leads to the cumulative loss of successive layers, i , of carbon atoms, from each of the six vertices for equi-vertex truncation, following the atomic layers series described above, that is 12, 24, 36, 54, 72, 96, 120, . . . , which again shows a rapid loss of atoms with increasing truncation. The total number of carbon atoms lost, where all vertices are equally truncated, is given by

$$N_{C,loss} = 6 \left\{ \sum_{k \text{ even}}^{\text{limit}} \frac{(i-k)[(i-k)+1]}{2} + \frac{i(i+1)}{2} \right\}, \quad (29)$$

where the upper ‘limit’ = $2[(i+2)/2 - 1]$. All of the above assume integer calculations adopting the lowest integer result in each case. In the octahedral diamondoid case truncation results in no net hydrogen atom loss if the truncated facets are hydrogen-passivated with CH₂ and CH groups. The CH _{n} group losses and gains, per vertex, are in this case

$$N_{CH_2,loss} = 1 \quad (30)$$

$$N_{CH_2,gain} = \left(\frac{i}{2} + 1 \right) \left\{ \frac{(i+1)}{2} + 1 \right\} \quad (31)$$

$$N_{CH,loss} = 2 N_{CH_2,gain} - 2 \quad (32)$$

$$N_{CH,gain} = 0. \quad (33)$$

The octahedral and truncated octahedral particle compositions are shown in Tables 5 and 6, respectively.

6.3. The spatial properties of diamond-bonded networks

In Fig. 7, we show the [CH]/[CH₂] ratios in diamond-bonded networks, of overall polyhedral form, as a function the number of constituent carbon atoms N_C . Perhaps the first thing of note is the wide spread in the ratios and, secondly, how the truncation of tetrahedral (T) networks can lead to exact and terminal octahedral particle (O) solutions (as noted in Sect. 5.4). The latter are reflected in the [CH]/[CH₂] ratios, that is the coincident red and blue squares on the thick blue line in Fig. 7. However, the reverse

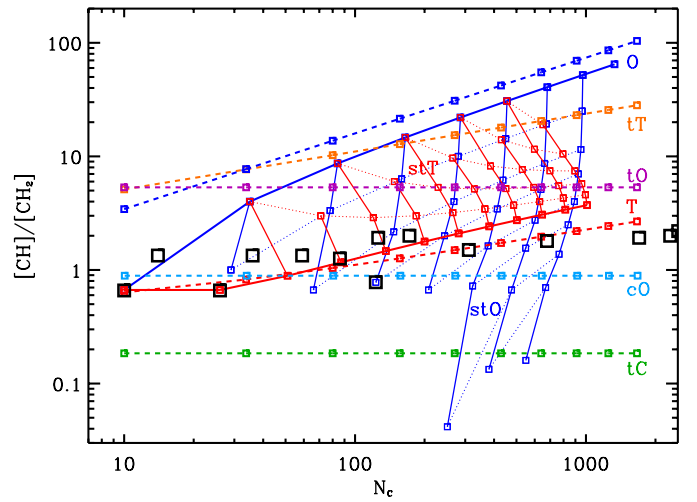


Fig. 7. CH/[CH₂] ratios in diamond-bonded networks of polyhedral form as a function of the truncation length (thin solid lines) increasing with distance from the thick solid red and blue lines, as a function of the number of constituent carbon atoms N_C : the thick solid lines are for the regular tetrahedral (red) and octahedral (blue) forms and the dangling and rising thinner lines show the effects of increasing truncation. The thick dashed lines show the [CH]/[CH₂] ratios for the polyhedral models: T (red), tT (orange), O (blue), tO (purple), cO (cobalt), and tC (green). For cubic particles (C) this ratio is zero. The data points show the only possible particle solutions with this truncation scheme. The black squares show the ratios for ‘spherical’ nano-diamonds for comparison.

is not true, in that octahedral particles cannot be truncated to exact tetrahedral forms and so there are no coincident solutions in this truncation direction and neither are there any truncated forms close to tetrahedral. In the latter case the truncated forms are truncated octahedron and cuboctahedron, as evidenced by the tendency of the truncated forms to flatter [CH]/[CH₂] ratios and to stray into the regions occupied by these polyhedra in Fig. 7.

For the network-modelled tetrahedral and octahedral nano-diamond particles, and their truncated forms, the [CH]/[CH₂] ratios are shown in Tables 3 to 6. Unlike the regular and semi-regular polyhedral modelling the diamond-bonded network is a discrete modelling process, in that only certain lattice-allowed dimensions are valid, as shown in Fig. 7 and the tables.

In comparing the T and O polyhedral forms with the tT and tO network forms it can clearly be seen that increasing T network truncation tends towards O polyhedra and O network truncation

Table 6. Truncated octahedral particle compositions.

i	N_C	N_H	n	$N_C(n)$	$N_H(n)$	N_{CH}	N_{CH_2}	N_{4°	H/C	X_H	[CH]/[CH ₂]
2	35	36	1	29	36	12	12	5	1.24	0.55	1.00
3	84	64	1	78	64	40	12	26	0.82	0.45	3.33
			2	66	64	16	24	26	0.97	0.49	0.67
4	165	100	1	159	100	76	12	71	0.63	0.39	6.33
			2	147	100	52	24	71	0.68	0.40	2.17
			3	123	100	28	36	59	0.81	0.45	0.78
5	286	144	1	280	144	120	12	148	0.51	0.34	10.00
			2	268	144	96	24	148	0.54	0.35	4.00
			3	244	144	72	36	136	0.59	0.37	2.00
			4	208	144	36	54	118	0.69	0.41	0.67
6	455	196	1	449	196	172	12	265	0.44	0.30	14.33
			2	437	196	148	24	265	0.45	0.31	6.17
			3	413	196	124	36	253	0.47	0.32	3.44
			4	377	196	88	54	235	0.52	0.34	1.63
			5	323	196	52	72	199	0.61	0.38	0.72
			6	251	196	4	96	151	0.78	0.44	0.04
7	680	256	1	674	256	232	12	430	0.38	0.28	19.33
			2	662	256	208	24	430	0.39	0.28	8.67
			3	638	256	184	36	418	0.40	0.29	5.11
			4	602	256	148	54	400	0.43	0.30	2.74
			5	548	256	112	72	364	0.47	0.32	1.56
			6	476	256	64	96	316	0.54	0.35	0.67
			7	380	256	16	120	244	0.67	0.40	0.13
8	969	324	1	963	324	300	12	651	0.34	0.25	25.00
			2	951	324	276	24	651	0.34	0.25	11.50
			3	927	324	252	36	639	0.35	0.26	7.00
			4	891	324	216	54	621	0.36	0.27	4.00
			5	837	324	180	72	585	0.39	0.28	2.50
			6	765	324	132	96	537	0.42	0.30	1.38
			7	669	324	84	120	465	0.48	0.33	0.70
			8	549	324	24	150	375	0.59	0.37	0.16

Notes. As a function of the number of atomic layers, i , and the number of atomic layer truncations, n . N_C and N_H are the total number of carbon and hydrogen atoms in the parent octahedron and $N_C(n)$ and $N_H(n)$ those in the truncated octahedron. N_{CH} and N_{CH_2} the number of CH_n groups on the surfaces, N_{4° the number of carbon atoms in the bulk and X_H the atomic hydrogen fraction.

tends towards, and indeed underpasses, tT polyhedra, tending towards tO and even underpassing tC polyhedra in some cases. Yet again, as can be seen in Fig. 7 this modelling clearly indicates that the nano-diamond [CH]/[CH₂] ratio likely varies over more than an order of magnitude for any given size particle.

Using the diamond network approach we constructed spherical nano-diamond particles of radius a_{nd} by filling the specified volume with a diamond lattice of a given number of C atoms, N_C , and then passivating the exposed surface atom dangling bonds with CH and CH₂ groups as required¹⁵. The particle properties and [CH]/[CH₂] ratios for these ‘spherical’ nano-diamonds are shown in Table 7 and Fig. 7 (black squares). We again point out that this is a discrete modelling process in that only certain particle dimensions are allowed, which is reflected in the values in the table because these data represent exact solutions to the filling of a given spherical volume with a regular diamond lattice. The black squares in Fig. 7 indicate that spherical nano-diamonds

would appear to have a rather narrow range in [CH]/[CH₂], that is from a value of 0.67 for adamantane (C₁₀H₁₆) up to ≈ 2.2 for particles with $N_C \leq 2500$. A close look at these data shows that spherical nano-diamonds exhibit [CH]/[CH₂] ratios approximating those of the tetrahedral polyhedral and network particles. This was indeed speculated by Pirali et al. (2007) who found that the [CH]/[CH₂] ratios of large diamondoid molecules or nano-diamonds ought to resemble those of the T_d point group, the largest subgroup of the O_h point group. We therefore concur with their speculation. Interestingly, the low [CH]/[CH₂] ratios for spherical nano-diamonds, would seem to imply that any (erosional) process that leads to a rounding of euhehedral/polyhedral nano-diamond facets would tend to suppress the [CH]/[CH₂] ratio, with respect to most non-cuboid polyhedral particle forms, if surface passivation with hydrogen is maintained.

7. The CH/CH₂ ratio in nano-diamonds as a ruler

The aim of this work is to explore whether it is possible to use the observed 3.53 $\mu\text{m}/3.43 \mu\text{m}$ (nano-)diamond IR band ratio as a

¹⁵ This approach ensures that there are no dangling bonds or pendant -CH₃ methyl groups.

Table 7. Spherical nano-diamond particle compositions.

Radius (nm)	N_C	N_H	N_{CH}	N_{CH_2}	$\frac{[CH]}{[CH_2]}$
0.27	10	16	4	6	0.67
0.31	14	20	8	6	1.34
0.36	26	32	8	12	0.67
0.40	36	40	16	12	1.34
0.44	59	60	24	18	1.34
0.53	123	100	28	36	0.78
0.76	311	178	76	151	1.50
0.98	678	296	140	78	1.80
1.33	1700	552	276	138	2.00
1.46	2316	694	340	177	1.92
1.51	2509	732	384	174	2.20
2.31	9177	1756	868	444	1.96
4.98	91 820	8160	4320	1920	2.25
8.99	539 011	26 556	14 400	6078	2.39

Notes. Theoretically-constructable nano-diamond structures with only surface CH and CH₂ groups, i.e. there are no pendant –CH₃ groups nor dangling bonds.

proxy for the ratio of the surface concentrations or abundances of CH and CH₂ groups, [CH]/[CH₂], on nano-diamonds, and hence as a ruler to measure their sizes in circumstellar (and interstellar) environments. Firstly, we need to consider whether the measured or observed 3.53 μ m and 3.43 μ m nano-diamond IR bands directly map the surface concentrations of CH and CH₂. This appears to be so but must be qualified because, although a direct mapping appears to be true for tetrahedral diamondoids, was shown by Pirali et al. (2007), this has not yet been demonstrated for larger species or for other (polyhedral) forms. Secondly, assuming that the direct mapping issue is a given, we need to determine if it is possible to use the ratio as a ruler. To this there can remain, as yet, no definitive answer within the astronomical context. This is because there is an inherent degeneracy in [CH]/[CH₂] between particle form and size. To break this degeneracy, or at least to reduce the uncertainties to a manageable degree, therefore requires some direct knowledge of the particle form and/or size. Currently, and if the nano-diamond form is unknown, a particular [CH]/[CH₂] ratio can spread over orders of magnitude in size (and the cube of this in mass!).

Clearly, it would help to have some idea of the form or the likely range of forms. As Pirali et al. (2007) have demonstrated, it appears that small diamondoids could tend towards tetrahedral forms for $N_C \leq 140$. While at the other size extreme, that is at micronic scales, images of synthetic nano-diamonds and CVD diamond coatings indicate that a wide range of particle shapes is possible, including: truncated octahedral (tO), cuboctahedral (cO), tetrahedral (T), and cubic (C) particles. Looking at these likely particle shapes, and the data presented in the figures here, it would therefore seem to be a lost cause to try and break the form/size degeneracy. For example, for the favoured tO and cO nano-particle forms the [CH]/[CH₂] ratio is, unfortunately, independent of size (see for example Figs. 2 and 7). Thus, it appears that a restriction to the tO and cO forms still does not sufficiently reduce the degeneracy to any useful degree because their [CH]/[CH₂] ratios are fixed in each case, independent of size, and are separated by about an order of magnitude (three orders of magnitude in mass)

In optical constant modelling it would seem that we therefore have little choice but to focus on a range of polyhedral forms, that is tetrahedral, truncated tetrahedral, octahedral, truncated

octahedral, and cuboctahedron (T, tT, O, tO, and cO). Ideally we could use the semi-regular forms stT and stO, to replace all of these but this approach would entail the introduction of the difficult to constrain truncation lengths, a , as free parameters into the mix. We would therefore like to be able to adopt a more restricted range of fixed forms, which can then be matched against the observed [CH]/[CH₂] values. Thus, it appears that the usual astronomical practice of assuming spherical particles is probably the most viable solution for nano-diamonds.

8. Stability and dehydrogenation considerations

Perhaps the first, and most fundamental, issue to be resolved is whether nano-diamonds actually are the most stable form of carbon at nano-scales. This was addressed by Badziag et al. (1990) who compared the heats of formation of small diamond and graphitic clusters. Following Nuth (1987a,b) these authors concluded that surface stabilisation plays a critical role and, consequently, that diamonds with hydrogen-terminated surfaces and radii smaller than ~ 1.5 nm are energetically favoured over polycyclic aromatics. However, since this early work the fullerene allotrope of carbon was discovered, which has added to the possible carbon nanoparticle forms that need to be considered. Barnard et al. (2003a) re-considered this issue, in the light of these more recent developments, and found that at the nanoscale diamond is not necessarily the most stable phase but that there is a ‘window’ of stability for nano-diamonds with radii ~ 0.9 – 2.6 nm ($1127 < N_C < 24\,398$). Further, Barnard et al. (2003a) found that fullerenes are the more stable form for smaller carbon clusters ($a < 0.9$ nm, $20 < N_C < 1127$), while graphite is the more stable form for larger clusters ($a > 2.6$ nm, $N_C > 24\,398$).

Nevertheless, the story does not end here because nano-diamonds are known to take several polyhedral forms, which have differing stability in their (de-)hydrogenated states (e.g. Barnard & Zapol 2004). This question was investigated in detail by Barnard & Zapol (2004) who found that, for hydrogenated nano-diamonds with $N_C > 10^4$ ($a \gtrsim 2.4$ nm) the cubic form is the most stable form, followed by the sphere, cuboctahedron or octahedron, and truncated octahedron. For dehydrogenated nano-diamonds the equivalent stability order is: truncated octahedron, cuboctahedron or sphere, octahedron, and cube but for smaller sizes the spherical form is the most stable with the cuboctahedron and truncated octahedron becoming more stable as size increases. For particles with up to 10^6 atoms ($a \leq 10$ nm), the dehydrogenated cubic and octahedral forms are higher in energy making them unlikely forms in the larger size range (Barnard & Zapol 2004). These shape- and size-dependent behaviours are principally due to the differences in the particle surface energies.

Given that in excited regions the nano-diamond surface hydrogenation may be less than complete, that is close to hot stars where they may undergo extreme heating and/or direct surface CH bond photo-dissociation, in our follow-up work we introduce a fractional surface H atom coverage factor, f_H , where $0 \leq f_H \leq 1$. A critical issue is then whether the different surface facets or, more generally, the different CH and CH₂ surface groups lose hydrogen atoms through the same processes and at the same rates.

A definitive answer to this is probably not yet possible but we can perhaps garner clues from some of the work published on the related issues of CH_{*n*} groups, surface re-structuring/relaxation, deprotonation potentials, and proton affinities (e.g. Zhigilei et al. 1997a,b; Barnard et al. 2003b; Barnard & Per 2014). The findings

of these works are consistent with other theoretical and experimental studies in this area. For instance, the theoretical work of [Barnard et al. \(2003b\)](#) shows, for dehydrogenated particles with $a \leq 0.5$ nm, that is less than a few hundred carbon atoms, that octahedral and cuboctahedral particle $\{111\}$ facets preferentially transform from sp^3 to sp^2 bonding, that is they exfoliate, resulting in onion-like structures with carbon clusters at their core ('bucky-diamonds'). They also found that $\{100\}$ (cubic) nano-diamonds are stable against exfoliation re-structuring.

Surface re-structuring must obviously have an effect on the CH_n surface group IR band strengths and positions. [Zhigilei et al. \(1997a,b\)](#) used classical molecular dynamics simulations to study diamond surface structural transformations of $\{111\}$ surfaces, designated $C\{111\}(1 \times 1)H$ structures in their terminology, which exhibit a single peak at $4.28 \mu\text{m}$ in their simulations. They explored the transformation of dehydrogenated bulk $\{111\}$ surfaces into $C\{111\}(2 \times 1)$ structures, that consist of π -bonded chains containing five- and seven-membered rings. With hydrogen adsorption, to form $C\{111\}(2 \times 1)H$ surfaces, an additional peak appears at $3.49 \mu\text{m}$ due to a metastable structure. As the hydrogen coverage in the simulations increases this peak increases in intensity, up to half monolayer coverage, and then disappears in favour of the $C\{111\}(1 \times 1)H$ $4.28 \mu\text{m}$ peak. They also found that $C\{111\}(2 \times 1)$ bulk surfaces graphitise upon heating to 2300 K.

In their later theoretical work ([Barnard & Per 2014](#)) studied the deprotonation potentials and proton affinities¹⁶ of ~ 0.9 – 1.4 nm radius nano-diamonds and found that they generally decrease with particle size but exhibit strong shape- and facet-dependencies. Differences of the order of 1 eV were found for 1 nm size variations and proton loss was found to be inhomogeneous over the nano-diamond surfaces. As [Barnard & Per \(2014\)](#) point out, tertiary ions ($\geq C^-$) being more stable than secondary ions ($> C < \overset{+}{H}$) results in tertiary (3°) CH bonds ($\geq C-H$) being more easily deprotonated than secondary CH bonds ($> C < \overset{+}{H}$) on facets, edges, and vertices. Thus, deprotonation, that is hydrogen abstraction or dehydrogenation by H^+ loss, occurs preferentially from facets. The opposing process, proton affinity, was found to be strongly facet-dependent while the deprotonation potential was edge/vertex-dependent. The proton affinity was found to be higher, that is protonation is preferred, on $\{110\}$ facets, followed by $\{111\}$ facets and then $\{100\}$ facets. From this work we can probably conclude that deprotonation (and by inference dehydrogenation) will tend to preferentially occur from tertiary CH on $\{111\}$ facets, while protons preferentially attach to, and therefore preferentially rehydrogenate, edges and vertices.

The theoretical and experimental observations described in the preceding paragraphs may be summarised into the following broad scenarios for the evolution of nano-diamond properties:

- *stability*: they are most stable for radii from 0.9 to 2.6 nm (for smaller [larger] sizes fullerenes [graphite] are more stable),
- *dehydrogenation*: occurs preferentially via the dissociation of 3° CH bonds on $\{111\}$ facets (before edges and vertices) leading to carbon atom sp^3 to sp^2 transformation (i.e. aromatisation),
- *re-structuring*: aromatisation triggers the formation of π -bonded chains with 5- and 7-membered rings and ultimately to outer layer exfoliation as edge-anchored, aromatic sheets that will shift absorption to longer (visible) wavelengths,
- *shape*: the preference for hydrogenated particles is: cube > sphere > cuboctahedron/octahedron > truncated octahedron. For

dehydrogenated particles the order is almost reversed but as their surfaces transform $sp^3 \rightarrow sp^2$ its relevance is moot, and

- *rehydrogenation*: occurs preferentially at edges and vertices, leading to a hysteresis with dehydrogenation because H atoms do not necessarily (re)attach to the sites they were removed from. The above summary indicates that modelling the thermal- and photo-processing of nano-diamonds in circumstellar regions must ideally try and include these complex surface re-structurations and compositional changes.

9. Discussion and speculations

The key parameters in determining the ratio of the CH and CH_2 IR band strengths are the surface structure, the euhedral (polyhedral) form and the edge to surface ratio where faces and/or edges exhibit different crystal facet properties. For example, regular tetrahedral (T), truncated tetrahedral (tT) and octahedral (O) particles (see [Fig. 1](#)) exhibit only $\{111\}$ facets and $\{111\}/\{111\}$ edges¹⁷ and their $[CH]/[CH_2]$ ratios are size-dependent and differ between the three polyhedral forms (see [Fig. 2](#)). In contrast, regular truncated octahedral (tO), cuboctahedral (cO), and truncated cubic (tC) particles exhibit both $\{111\}$ and $\{100\}$ facets and $\{111\}/\{100\}$ edges, and also $\{111\}/\{111\}$ edges in the case of tO ([Fig. 1](#)). However, the $[CH]/[CH_2]$ ratios for these particles do not depend on size and are spread over more than an order of magnitude ([Fig. 2](#)). For cubic (C) particles the $[CH]/[CH_2]$ ratio is zero because they exhibit no tertiary CH bonds on their exclusively $\{100\}$ surfaces.

For fully surface-hydrogenated nano-diamonds larger than typical diamondoids (e.g. $N_C > 100$) the most stable, and therefore the most likely, forms are the cube (C), followed by the sphere, cuboctahedron(cO)/octahedron(O), and truncated octahedron (tO) ([Barnard & Zapol 2004](#)). For the cube $[CH]/[CH_2] = 0$ and so is of no help to us here, even though it may be the most stable form. Of the remaining four only two exhibit size-dependent $[CH]/[CH_2]$ ratios, the sphere because it mimics tetrahedral particles (see [Sect. 5.4](#)) and the octahedron (O). The $[CH]/[CH_2]$ ratios for the cuboctahedron (cO) and truncated octahedron (tO) are fixed at ~ 0.9 and ~ 5.3 , respectively.

[Figure 8](#) summarises the $[CH]/[CH_2]$ ratios for all of the modelled polyhedra and network structures, the data are the same as in the previous figures but are here plotted as a function of the equivalent sphere radius, a_{nd} , rather than against the number of carbon atoms, N_C . These are compared with the typical range (0.5–3) for the experimental and observational data (grey shaded area). From this figure we conclude that, for particles with radii larger than ~ 1 nm, only spherical nano-diamonds (black squares) and truncated octahedral/cuboctahedral nano-diamonds in their semi-regular forms ('vertical' blue lines) appear to be consistent with the measured data. However, for nano-diamonds with radii smaller than ~ 1 nm it appears that almost any shape could be consistent with the data. Thus, from a consideration of the $[CH]/[CH_2]$ ratio it seems that spherical and truncated octahedral/cuboctahedral nano-diamonds are the most probable forms. It is interesting that [Barnard & Zapol \(2004\)](#) basically come to the same conclusion but from a completely different and energetic point of view. Thus, and given that

¹⁶ The deprotonation energy is the enthalpy change of the reaction nano-diamond-H \rightleftharpoons nano-diamond⁻ + H^+ .

The proton affinity is the negative of the enthalpy change of the reaction nano-diamond + H^+ \rightleftharpoons nano-diamond-H⁺.

¹⁷ However, it should be noted that not all $\{111\}/\{111\}$ edges are equivalent. For example, these edges are lined with CH_2 groups on tetrahedral particles but with CH groups on octahedral particles, the CH groups in the latter case actually being an integral part of the adjacent facets.

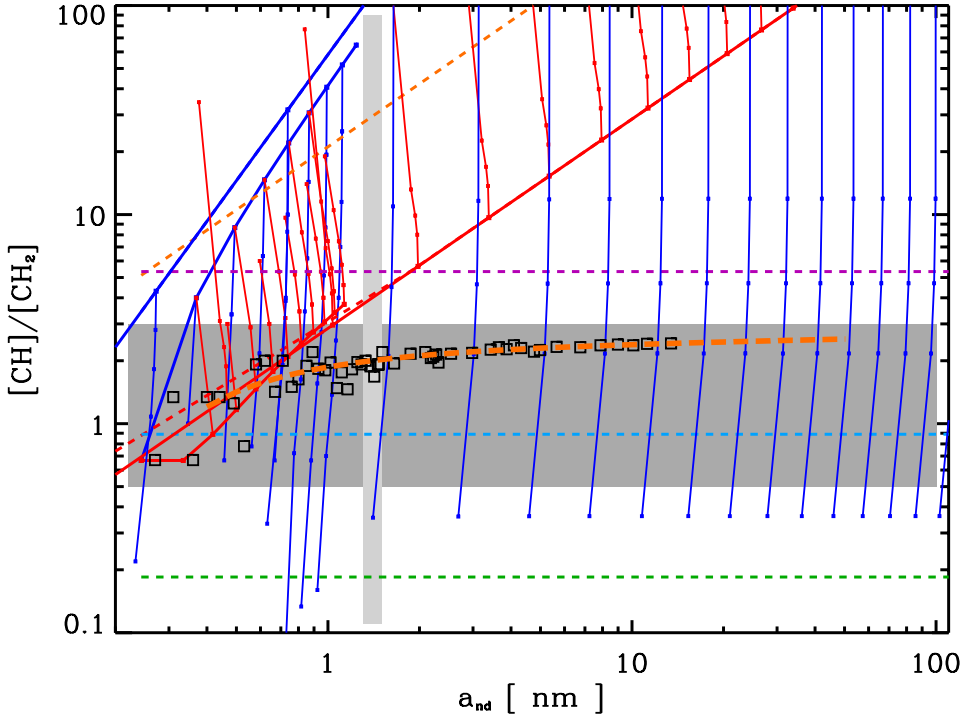


Fig. 8. Ranges of the $[\text{CH}]/[\text{CH}_2]$ ratios for all of the considered models: tetrahedra and octahedra including their truncated forms, solid red and blue lines, respectively. The dangling and rising thinner lines show the effects of increasing truncation. The dashed lines show the $[\text{CH}]/[\text{CH}_2]$ ratios for the regular polyhedra: T (red), tT (orange), O (blue), tO (purple), cO (cobalt), and tC (green). For cubic particles (C) this ratio is zero. The black squares show the ratios for ‘spherical’ nano-diamonds and the orange dashed line shows an analytical approximation to these data (see text for details). The grey shaded gives an indication of the observed and experimental values (0.5–3) and the lighter grey vertical band indicates the typical radii of the most abundant pre-solar nano-diamonds (1.3–1.5 nm).

regular tetrahedral (T) and octahedral (O) forms are apparently not favoured, nano-diamonds in astrophysical environments must therefore include spherical, semi-regular and truncated octahedral family (cO, tO and stO) particle forms in order to allow for the observed variations in the CH to CH₂ band ratio both in the laboratory and in space (see Fig. 8 and also Sects. 4.8 and 5.4 for a discussion of these effects).

Determining nano-diamond sizes, both in space and in the laboratory, from only their 3–4 μm spectra will be difficult unless the particle shapes are well-determined. Therefore, an increase in useful information, such as further laboratory data and the modelling of any specific nano-diamond bands at longer wavelengths, is critical for interpreting their spectra with future instruments, such as the *James Webb Space Telescope* (JWST), that will give us a more complete spectral coverage than currently available. However, it is likely that most longer wavelength (i.e. mid-IR) bands are due to (nitrogen) hetero-atom impurity and structural defects in diamond (e.g. Hill et al. 1998; Jones & d’Hendecourt 2000; Braatz et al. 2000) and so may not be particularly size-diagnostic.

Nevertheless, the spherical nano-diamond data do indicate an apparent convergence in the $[\text{CH}]/[\text{CH}_2]$ ratio (to ≈ 2.4) for the larger sizes (see Fig. 8). However, at the smaller (actual) sizes ($a_{\text{nd}} \leq 10$ nm), as shown in Fig. 9), there is an inherent and unavoidable dispersion in the CH_n group abundance data, which is due to trying to shoehorn a discretised, 3D diamond network lattice into a volume imposed by a given radius¹⁸. The red line in Fig. 9 (and the long-dashed orange line in Fig. 8) is a by-eye fit to these data with the following function

$$\frac{[\text{CH}]}{[\text{CH}_2]} = 2.265 a_{\text{nd}}^{0.03} - \left(\frac{1}{2.5 a_{\text{nd}}} \right), \quad (34)$$

where the nano-diamond radius a_{nd} is in nm. This equation may thus provide a means to avoid the ‘ups and downs’ in determining the $[\text{CH}]/[\text{CH}_2]$ ratio by exact diamond network

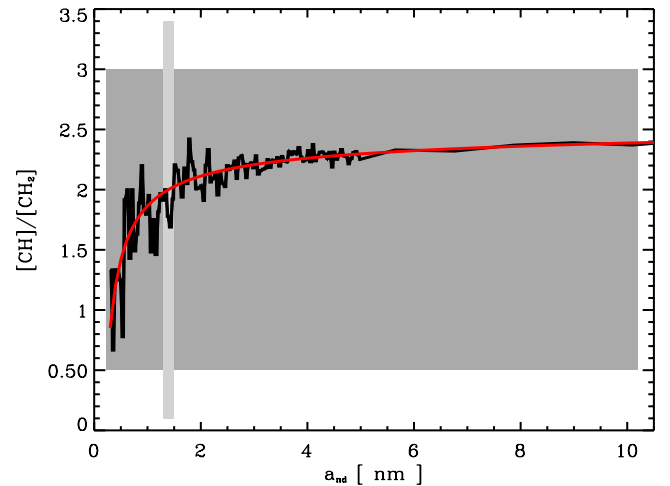


Fig. 9. $[\text{CH}]/[\text{CH}_2]$ ratios for ‘spherical’ nano-diamonds with actual radii ≤ 10 nm (black line), showing the inherent dispersion in the data. The red line shows the analytical approximation to these data (see text for details). The grey shaded gives an indication of the observed and experimental values (0.5–3) and the lighter grey vertical band indicates the typical radii of the most abundant pre-solar nano-diamonds (1.3–1.5 nm).

calculations (see Fig. 9), which introduce unpredictable ‘noise’ into the derivation. In essence, Eq. (34) therefore provides a sort of statistical averaging of the $[\text{CH}]/[\text{CH}_2]$ ratios and may yield a means of estimating nano-diamond sizes from their IR spectra. Even though Eq. (34) is only indicative it does show that, if circumstellar nano-diamonds are quasi-spherical, there may be some hope in estimating the sizes of the larger nano-diamonds ($a_{\text{nd}} \gtrsim 2$ nm) from their $[\text{CH}]/[\text{CH}_2]$ ratios, albeit with some uncertainty because of the rather flat dependence of $[\text{CH}]/[\text{CH}_2]$ on radius. The utility of such a simple expression clearly rests upon adopting the critically fundamental assumption of spherical nano-diamonds. Unfortunately, given the wide dispersion in

¹⁸ In the diamond network calculations here the actual particle radius is determined by the structure discretisation and not by the imposed radius.

their properties, the sizes and shapes of circumstellar (and interstellar?) nano-diamonds with radii $\lesssim 2$ nm are probably always going to be somewhat poorly constrained by their $[\text{CH}]/[\text{CH}_2]$ ratios.

The survivability of nano-diamonds in intense radiation fields close to bright stars is determined by their absorption of energetic (UV to EUV) photons versus their ability to shed this absorbed energy via thermal emission, be it through stochastic or thermal equilibrium emission. The nano-diamond surface-to-volume ratio and also the nature of the particle surfaces, in particular the degree of surface hydrogenation, are critical in determining the absolute balance between absorption and emission. In this sense, smaller nano-diamonds have both high surface-to-volume ratios and high surface hydrogen atom fractions and are, perhaps paradoxically, more resilient than their larger relations. While larger, fully hydrogenated nano-diamonds will be more stable than in their de-hydrogenated forms, if they were to lose their surface hydrogen through extreme heating they would undergo surface aromatisation and likely runaway heating leading to their rapid erosion and destruction.

At large distances from bright stars fully-hydrogenated nano-diamonds of all sizes should be stable against extreme thermal processing. Nevertheless, given that the analysed pre-solar nano-diamonds are the most abundant of all pre-solar grains and have approximately log-normal size distributions peaking at diameters $\phi \approx 3$ nm and extending out to $\phi \sim 10$ nm (Lewis et al. 1987, 1989; Daulton et al. 1996), it would seem that nano-diamonds with radii as large as 100 nm are not the norm. Indeed, it appears that the pre-solar nano-diamond sizes fall well within the nano-diamond stability window ($\phi = 1.9\text{--}5.2$ nm, Barnard et al. 2003a). If large nano-diamonds were common we would surely see signs of them in the pre-solar grains but we do not. A possible explanation for this is that the nano-diamonds are actually formed in the inner regions of circumstellar regions, by some as yet unspecified process¹⁹, and that they are there size-sorted as a result of thermal processing, which leads to the observed size distribution biased towards smaller nano-diamonds. Indeed we know that the analysed pre-solar nano-diamonds, or at least some fraction of them, must be of extra-solar origin based upon their anomalous Xe isotopic component (Xe-HL), which is considered characteristic of the nucleosynthetic processes in supernovae (Lewis et al. 1987). This extra-solar origin is also supported by the fact that they exhibit ¹⁵N depletions and low C/N ratios that are consistent with carbon-rich stellar environments (Alexander 1997).

There has always been something of a question mark over the origin of the anomalous Xe-HL in pre-solar nano-diamonds. It has been proposed that it arises from implantation (e.g. Verchovsky et al. 2000). However, it is hard to understand how this process could lead to the trapping of Xe atoms in such small particles, when it would be expected that the incident heavy, Xe ions would likely traverse the particle rather than be implanted. If small nano-diamonds are, however, formed by the erosion of much larger particles in intense radiation field environments, it is possible that the heavier Xe atoms could be retained in the grain during down-sizing as a result of progressive sublimation. Such an effect would, as required, explain Xe atom trapping in nano-diamonds and also result in a concentration effect that would increase the number of Xe atoms per unit nano-diamond mass.

Taking the Xe-HL to carbon ratio in nano-diamonds, $f(\frac{\text{Xe}}{\text{C}})_{\text{nd}}^{\odot}$, to be 1.7×10^{-3} of the solar ratio (Anders & Zinner

1993), the solar abundances of xenon, $[\text{Xe}]_{\odot} = 1.9 \times 10^{-10}$, and of carbon, $[\text{C}]_{\odot} = 3.2 \times 10^{-4}$ (Palme et al. 2014), we can estimate the quantity of cosmic carbon likely tied up in nano-diamonds. Given that the most abundant pre-solar nano-diamonds have radii ≈ 1.5 nm and $\sim 2,500$ carbon atoms per grain ($N_{\text{C,nd}}$, see Table 7) then the fraction of nano-diamonds that contain a Xe-HL atom, f_{Xe} , is

$$\begin{aligned} f_{\text{Xe}} &= \frac{[\text{Xe}]}{[\text{C}]} f\left(\frac{\text{Xe}}{\text{C}}\right)_{\text{nd}}^{\odot} N_{\text{C,nd}} = \frac{1.9 \times 10^{-10}}{3.2 \times 10^{-4}} \times 1.7 \times 10^{-3} \times 2500 \\ &= 2.5 \times 10^{-6}, \end{aligned} \quad (35)$$

which implies that only one in 400 000 nano-diamonds actually contains a xenon atom. From this we can conclude that there must, inescapably, be a large reservoir of pre-solar nano-diamonds that are Xe-free but must be associated with the nano-diamonds that do contain Xe atoms, that is all of these other nano-diamonds are ‘guilty by association’ and have to come from the same source or sources.

Expressing this in another way the fraction of solar carbon that must be associated with the Xe-containing pre-solar nano-diamonds, $f_{\text{C,nd}}$, can be estimated from the Xe/C ratio in nano-diamonds with respect to the solar Xe/C ratio $f(\frac{\text{Xe}}{\text{C}})_{\text{nd}}^{\odot}$ ($= 0.0017$) (Anders & Zinner 1993), which is equivalent to $\approx 0.2\%$ of the solar carbon abundance. Given that the heavy Xe atom trapping efficiency into nanoparticles, f_{trap} , by whatever mechanism, cannot be a very efficient process ($f_{\text{trap}} < 1$) the actual fraction of carbon tied up in nano-diamonds in circumstellar and interstellar media must be significantly larger, that is $f_{\text{C,nd}} > 0.2\%$. In their experiments Koscheev et al. (2001) found that the efficiency for He, Ne, Kr, and Xe atom trapping into nano-diamonds is of the order of 10%, which implies that $f_{\text{C,nd}}$ must be at least of the order of 2%. If the origin of the Xe-HL atoms is by implantation at keV energies, then this inefficiency is compounded by the experimental observation that nano-diamonds with radii less than ~ 4 nm can be completely destroyed during the Xe implantation process (Shiryaev et al. 2018). Consequently the Xe record would be preferentially preserved in the larger size fraction of the pre-solar nano-diamonds. This experimental result is a further indication of the inefficient trapping of Xe atoms in nano-diamonds. The initial nano-diamond reservoir must therefore have been considerably larger than that indicated by the measured Xe content, implying that $f_{\text{C,nd}} > 2\%$ or, given that $\approx 50\%$ of carbon is in dust, that $> 4\%$ of the cosmic carbonaceous dust ought to be in the form of nano-diamonds. Thus, if a significant fraction of them are indeed interstellar, as well as circumstellar, as is an unavoidable conclusion given that a significant fraction were associated with distant supernovae and have therefore traversed the interstellar medium, then it would seem that they have to be ‘multi-talented’²⁰ and well hidden with(in) other (carbon) dust components in order to have avoided widespread detection in interstellar and circumstellar media.

10. Summary and conclusions

We developed several different approaches to the calculation of the CH and CH₂ group abundances on nano-diamonds: regular and semi-regular polyhedral shapes, and diamond bonding

²⁰ Nano-diamonds in the ISM would have to express their presence in multiple, but indirect, ways in order to most efficiently use the rather limited supply of carbon available (e.g. Jones & d’Hendecourt 2000), i.e. they would have to contribute to the FUV extinction, the 3–15 μm IR emission bands, the mid-IR emission, ...

¹⁹ As noted by Daulton et al. (1996), the pre-solar nano-diamonds were most probably formed via some vapour phase condensation process.

networks. As a function of the particle size and shape, and for the different calculation methods, we derived the relative abundance ratio [CH]/[CH₂], which can then be weighted by the laboratory-measured IR band intensity ratio in order to interpret and/or predict the observed 3.53 μm/3.43 μm (nano-)diamond IR band ratio. We found that the various methods give good qualitative agreement, within the likely uncertainties.

Overall we found that the [CH]/[CH₂] ratio, and therefore the observed IR band intensity ratios, ought to strongly depend upon both the particle size and shape. For a given particle size or shape the [CH]/[CH₂] ratio varies over more than an order of magnitude. Thus, it appears that it will be somewhat difficult to constrain the sizes of the observed nano-diamonds solely on the basis of their observed infrared spectra in the 3–4 μm region. This conclusion remains valid even if we restrict ourselves to the most probable and most stable nano-diamonds forms, that is spherical and the family of cO, tO, and stO (cuboctahedral and truncated octahedral) particles.

If we, justifiably, make the strong assumption that circumstellar (and interstellar) nano-diamonds are (quasi-)spherical, then there may be some hope in estimating the sizes of nano-diamonds larger than ≈2 nm from the observed ratios of the CH and CH₂ IR bands at 3.53 μm and 3.43 μm, respectively. Although, the uncertainties are still likely to be rather large because of the very flat dependence of their [CH]/[CH₂] ratio on radius ($\propto a_{\text{nd}}^{0.03}$). If this same statistically-averaged, size-dependent behaviour is assumed to hold for the smallest nano-diamonds ($a_{\text{nd}} < 10$ nm) then we may have some hope estimating their mean sizes, with the critical caveat that the surfaces are fully hydrogenated and/or that de-hydrogenation processes do not affect the surface CH and CH₂ groups abundance ratios.

Further laboratory and modelling data of the longer wavelength (mid-IR) bands specific to nano-diamonds is therefore essential for the coming JWST era if we are to understand and extract the maximum amount of data from circumstellar nano-diamond spectra. With these new spectroscopic data, we will perhaps discover nano-diamonds in new astronomical objects, other than circumstellar discs regions, and that they even exist in the interstellar medium. Although, and as a caveat, it is probable that as interesting as these bands will be they may not be particularly size-specific because they are predominantly, and perhaps exclusively, due to impurities such as nitrogen and to structural defects in the diamond lattice.

As something of an aside, based upon their hetero-atom Xe content, it is here speculated that nano-diamonds may actually be quite abundant in the ISM; of the order of several percent of cosmic carbon could be in the form of nano-diamonds. However, given that they have not yet been detected there they must be well-hidden with(in) other dust components, either that or we do not yet recognise their spectroscopic signatures in the ISM because they are confused with other carbonaceous dust features.

Interestingly, this modelling indicates that spherical nano-diamonds exhibit a narrower range in [CH]/[CH₂] than shown by the regular and semi-regular polyhedral forms and also by the polyhedral nano-diamond network models. Further, spherical nano-diamonds exhibit [CH]/[CH₂] ratios approximating those of the tetrahedral polyhedral and network particles, as has already been speculated, that is the ratios for large diamondoid molecules or nano-diamonds resemble those of the T_d point group, the largest subgroup of the O_h point group.

Acknowledgements. The author particularly wishes to thank Nathalie Ysard for a very careful reading of the manuscript and an extremely thorough and

painstaking verification of the equations. The author is especially grateful to the anonymous referee for the critical suggestions that led to a fundamental clarification of the presentation. This work is dedicated to Keith, my long-suffering brother of more than 63 yr. Taken from us too soon he will remain forever in our hearts and minds. Keith Edward Jones (25 February 1957–29 October 2020).

References

- Alexander, C. M. O. 1997, in *AIP Conf. Ser.*, **402**, eds. T. J. Bernatowicz, & E. Zinner, 567
- Allamandola, L. J., Sandford, S. A., Tielens, A. G. G. M., & Herbst, T. M. 1992, *ApJ*, **399**, 134
- Anders, E., & Zinner, E. 1993, *Meteoritics*, **28**, 490
- Andersen, A. C., Jorgensen, U. G., Nicolaisen, F. M., Sorensen, P. G., & Glejbol, K. 1998, *A&A*, **330**, 1080
- Badziag, P., Verwoerd, W. S., Ellis, W. P., & Greiner, N. R. 1990, *Nature*, **343**, 244
- Barnard, A. S., Per, M. C. 2014, *Nanotechnology*, **25**, 445702
- Barnard, A. S., & Sternberg, M. 2005, *J. Phys. Chem. B*, **109**, 17107
- Barnard, A. S., & Zapol, P. 2004, *J. Chem. Phys.*, **121**, 4276
- Barnard, A. S., Russo, S. P., & Snook, I. K. 2003a, *J. Chem. Phys.*, **118**, 5094
- Barnard, A. S., Russo, S. P., & Snook, I. K. 2003b, *Diamond Related Mater.*, **12**, 1867
- Braatz, A., Ott, U., Henning, T., Jäger, C., & Jeschke, G. 2000, *Meteor. Planet. Sci.*, **35**, 75
- Brooke, T. Y., Sellgren, K., & Smith, R. G. 1996, *ApJ*, **459**, 209
- Chen, C. F., Wu, C. C., Cheng, C. L., Sheu, S. Y., & Chang, H. C. 2002, *J. Chem. Phys.*, **116**, 1211
- Colangeli, L., Mennella, V., Stephens, J. R., & Bussoletti, E. 1994, *A&A*, **284**, 583
- Daulton, T. L., Eisenhour, D. D., Bernatowicz, T. J., Lewis, R. S., & Buseck, P. R. 1996, *Geochim. Cosmochim. Acta*, **60**, 4853
- Guillois, O., Ledoux, G., & Reynaud, C. 1999, *ApJ*, **521**, L133
- Habart, E., Testi, L., Natta, A., & Carillet, M. 2004, *ApJ*, **614**, L129
- Hill, H. G. M., Jones, A. P., & D'Hendecourt, L. B. 1998, *A&A*, **336**, L41
- Huss, G. R., & Lewis, R. S. 1995, *Geochim. Cosmochim. Acta*, **59**, 115
- Jones, A. P. 2012a, *A&A*, **540**, A1
- Jones, A. P. 2012b, *A&A*, **540**, A2; erratum: *A&A*, **545**, C2
- Jones, A. P. 2012c, *A&A*, **542**, A98; erratum: *A&A*, **545**, C3
- Jones, A. P., & d'Hendecourt, L. 2000, *A&A*, **355**, 1191
- Jones, A. P., D'Hendecourt, L. B., Sheu, S.-Y., et al. 2004, *A&A*, **416**, 235
- Jones, A. P., Köhler, M., Ysard, N., Bocchio, M., & Verstraete, L. 2017, *A&A*, **602**, A46
- Kimoto, S., Dick, W. D., Syedain, Z., Pui, D. Y. H., & Roberts, D. L. 2014, *International Aerosol Conference*
- Koike, C., Wickramasinghe, N. C., Kano, N., et al. 1995, *MNRAS*, **277**, 986
- Koscheev, A. P., Gromov, M. D., Mohapatra, R. K., & Ott, U. 2001, *Nature*, **412**, 615
- Lewis, R. S., Ming, T., Wacker, J. F., Anders, E., & Steel, E. 1987, *Nature*, **326**, 160
- Lewis, R. S., Anders, E., & Draine, B. T. 1989, *Nature*, **339**, 117
- Mutschke, H., Dorschner, J., Henning, T., Jäger, C., & Ott, U. 1995, *ApJ*, **454**, L157
- Mutschke, H., Andersen, A. C., Jäger, C., Henning, T., & Braatz, A. 2004, *A&A*, **423**, 983
- Nuth, J. A., III 1987a, *Ap&SS*, **139**, 103
- Nuth, III, J. A. 1987b, *Nature*, **329**, 589
- Palme, H., Lodders, K., & Jones, A. 2014, *Solar System Abundances of the Elements*, ed. A. M. Davis, 15
- Pirali, O., Vervloet, M., Dahl, J. E., et al. 2007, *ApJ*, **661**, 919
- Reich, K. V. 2011, *JETP Lett.*, **94**, 22
- Sheu, S.-Y., Lee, I. P., Lee, Y. T., & Chang, H.-C. 2002, *ApJ*, **581**, L55
- Shiryaev, A. A., Hinks, J. A., Marks, N. A., et al. 2018, *Sci. Rep.*, **8**, 5099
- Steglich, M., Huisken, F., Dahl, J. E., Carlson, R. M. K., & Henning, T. 2011, *ApJ*, **729**, 91
- Usoltseva, L. O., Volkov, D. S., Nedosekin, D. A., et al. 2018, *Photoacoustics*, **12**, 55
- Van Kerckhoven, C., Tielens, A. G. G. M., & Waelkens, C. 2002, *A&A*, **384**, 568
- Verchovsky, A. B., Wright, I. P., & Pillinger, C. T. 2000, in *Lunar Planet. Sci. Conf.*, 1804
- Zhigilei, L. V., Srivastava, D., & Garrison, B. J. 1997a, *Phys. Rev. B (Condensed Matter)*, **55**, 1838
- Zhigilei, L. V., Srivastava, D., & Garrison, B. J. 1997b, *Surf. Sci.*, **374**, 333

Appendix A: Regular polyhedral particles

Here we consider all of the relevant equations pertaining to regular and regular truncated polyhedral particles where all particle edges are of length, l . Following the modelling of regular and semi-regular polyhedra and their truncated forms presented in this work we propose the following rules, which generalise the observations presented in Section 3, for determining the CH_n group terminations of nano-diamond polyhedral vertices, edges, and facets:

- Vertices (V)
 - with an even number of intersecting facets are CH_2 ,
 - with an odd number of intersecting {111} facets are CH,
 - with one or more intersecting {100} facets are CH_2 ,
- Edges (E)
 - between facets of the same type are CH_2 ,
 - of triangular facets are CH_2 ,
 - between a square and a hexagonal facet are CH,
- Facets (F)
 - with three and six sides are {111},
 - with four and eight sides are {100},
 - {111} are covered in coherently-directed CH bonds and
 - {100} are CH_2 covered.

These rules can be used to determine the CH_n group structures comprising the surfaces of polyhedral nano-diamonds.

Appendix A.1: Regular tetrahedral (T) particles

We first describe the properties of regular tetrahedral particles, the simplest regular polyhedra, where the total edge length is $6l$ (see Fig. 1 and Tables 1 and 2). An encompassing sphere, that is one that is equally arrayed around and intersects all four of the particle vertices, is of radius $r = \sqrt{6/4}l = 0.612l$. The surface area of a tetrahedron, with four equivalent, triangular {111} facets, each of area $\sqrt{3}/4 l^2$, is:

$$A_T = \sqrt{3} l^2 = \sqrt{3} \left(\frac{4}{\sqrt{6}} \right)^2 r^2 = \frac{8\sqrt{3}}{3} r^2 = 4.619 r^2. \quad (\text{A.1})$$

Given that the entire surface area is in {111} facets, $f_{s\{111\}} = 1$, which does not include the four CH-terminated vertices. All edges are distinct in structure from the faces, are CH_2 -terminated and can be considered to be of {100}-type with a {100} edge length $E_{\{100\}} = 6l = 4\sqrt{6}r = 9.798r$. The ratio of the total edge length, E_T , to the total surface area of such a particle is

$$\frac{E_T}{A_T} = \frac{6l}{\sqrt{3} l^2} = \frac{2\sqrt{3}}{l} = \frac{3\sqrt{2}}{2r} = \frac{2.121}{r} \quad (\text{A.2})$$

and the ratio of the surface area of a tetrahedron to that of its encompassing sphere is

$$\frac{A_T}{A_{\text{sphere}}} = \frac{8\sqrt{3}/3 r^2}{4\pi r^2} = \frac{2}{\pi\sqrt{3}} = 0.368. \quad (\text{A.3})$$

The volume of a tetrahedron is given by:

$$V_T = \frac{\sqrt{2}}{12} l^3 = \frac{\sqrt{2}}{12} \left(\frac{4}{\sqrt{6}} \right)^3 r^3 = \frac{8}{9\sqrt{3}} r^3 = 0.513 r^3 \quad (\text{A.4})$$

and the ratio of the volume of a tetrahedron to that of its encompassing sphere is:

$$\frac{V_T}{V_{\text{sphere}}} = \frac{[8\sqrt{3}/9] r^3}{(4/3)\pi r^3} = \frac{2}{\pi 3\sqrt{3}} = 0.123. \quad (\text{A.5})$$

Hence, and because for convenience we usually define the particle mass in terms of a radius, the volume of a tetrahedron, with circumscribed sphere of effective radius r_{eff} , must be normalised to that of a spherical particle of the same volume $V_T(r_{\text{eff}})$, that is the radius, a_{nd} , of a "spherical nano-diamond" is defined by

$$\frac{4}{3}\pi a_{\text{nd}}^3 = \frac{8}{9\sqrt{3}} r_{\text{eff}}^3 \quad (\text{A.6})$$

and hence

$$r_{\text{eff}} = \left(\frac{\pi 3\sqrt{3}}{2} \right)^{\frac{1}{3}} a_{\text{nd}} = 2.103 a_{\text{nd}}. \quad (\text{A.7})$$

We note that r_{eff} is greater than a_{nd} because any polyhedron is, individually, less efficient at space filling than a sphere.

Appendix A.2: Regular truncated tetrahedral (tT) particles

In the same manner as for tetrahedral particles we now look to the equivalent properties of regular truncated tetrahedral particles, that is tetrahedral particles with the four vertices truncated into equilateral triangular faces. In this case the total edge length is $18l$ (see Fig. 1 and Tables 1 and 2) and the encompassing sphere radius $r = \sqrt{22/4}l = 1.173l$. The surface area of a truncated tetrahedron, with four equivalent, triangular {111} facets (each of area $\sqrt{3}/4 l^2$), and four hexagonal {100} facets each of area $3\sqrt{3}/2 l^2$, is:

$$A_{tT} = 7\sqrt{3} l^2 = 7\sqrt{3} \left(\frac{4}{\sqrt{22}} \right)^2 r^2 = \frac{56\sqrt{3}}{11} r^2 = 8.818 r^2. \quad (\text{A.8})$$

Given that the entire surface area is in triangular and hexagonal {111} facets, $f_{s\{111\}} = 1$. However, unlike tetrahedra, not all edges are {100}-type, twelve are CH-terminated and therefore an integral part of the adjacent {111} facets. Thus, only six of the truncated form edges are of {100} CH_2 -type and $E_{\{100\}} = 6l = (24/\sqrt{22})r = 5.117r$. The ratio of the total edge length, E_{tT} , to the total surface area of such a particle is

$$\frac{E_{tT}}{A_{tT}} = \frac{18l}{7\sqrt{3} l^2} = \frac{6\sqrt{3}}{7l} = \frac{3\sqrt{3}\sqrt{22}}{14r} = \frac{1.741}{r} \quad (\text{A.9})$$

and the ratio of the surface area to that of the encompassing sphere is

$$\frac{A_{tT}}{A_{\text{sphere}}} = \frac{56\sqrt{3}/11 r^2}{4\pi r^2} = \frac{14\sqrt{3}}{11\pi} = 0.702. \quad (\text{A.10})$$

The volume of a truncated tetrahedron is given by:

$$V_{tT} = \frac{23\sqrt{2}}{12} l^3 = \frac{23\sqrt{2}}{12} \left(\frac{4}{\sqrt{22}} \right)^3 r^3 = \frac{184}{33\sqrt{11}} r^3 = 1.681 r^3 \quad (\text{A.11})$$

and the ratio of the volume of a truncated tetrahedron to that of its encompassing sphere is:

$$\frac{V_{tT}}{V_{\text{sphere}}} = \frac{[184/(33\sqrt{11})] r^3}{(4/3)\pi r^3} = \frac{46}{\pi 11\sqrt{11}} = 0.401. \quad (\text{A.12})$$

Normalising to a spherical particle of the same volume $V_{\text{tetra.}}(r_{\text{eff}})$, the radius, a_{nd} , of the equivalent "spherical nano-diamond" is from

$$\frac{4}{3}\pi a_{\text{nd}}^3 = \frac{184}{33\sqrt{11}} r_{\text{eff}}^3 \quad (\text{A.13})$$

whence

$$r_{\text{eff}} = \left(\frac{\pi 11\sqrt{11}}{46} \right)^{\frac{1}{3}} a_{\text{nd}} = 1.356 a_{\text{nd}}. \quad (\text{A.14})$$

Appendix A.3: Regular octahedral (O) particles

We now consider the properties of regular octahedral particles, with a total edge length of $12l$ (see Fig. 1 and Tables 1 and 2) and an encompassing sphere of radius $r = \sqrt{2}/2l = 0.707l$. The surface area of an octahedron, which exhibits eight equivalent triangular $\{111\}$ facets is:

$$A_O = 8 \frac{\sqrt{3}}{4} l^2 = 2\sqrt{3} \left(\frac{2}{\sqrt{2}} \right)^2 r^2 = 4\sqrt{3} r^2 = 6.928 r^2. \quad (\text{A.15})$$

As per tetrahedral particles, the surface of octahedral particles is entirely in triangular $\{111\}$ facets, that is $f_{s\{111\}} = 1$. However, in this case, all the $\{111\}/\{111\}$ edges are comprised of alternately-facing CH bonds forming an integral part of those adjacent facets.²¹ Hence, $E_{\{100\}} = 0$ and the total edge length $E_O = 12l = 12\sqrt{2}r = 16.971r$. The ratio of the total edge length, E_O , to the total surface area of such a particle is

$$\frac{E_O}{A_O} = \frac{12l}{2\sqrt{3}l^2} = \frac{2\sqrt{3}}{l} = \frac{2\sqrt{3}\sqrt{2}}{2r} = \frac{\sqrt{6}}{r} = \frac{2.450}{r}. \quad (\text{A.16})$$

The ratio of the surface area to that of its encompassing sphere is

$$\frac{A_O}{A_{\text{sphere}}} = \frac{4\sqrt{3}r^2}{4\pi r^2} = \frac{\sqrt{3}}{\pi} = 0.551. \quad (\text{A.17})$$

The volume of an octahedron is

$$V_O = \frac{\sqrt{2}}{3} l^3 = \frac{\sqrt{2}}{3} \left(\frac{2}{\sqrt{2}} \right)^3 r^3 = \frac{4}{3} r^3 = 1.333 r^3 \quad (\text{A.18})$$

and the ratio of its volume to that of the encompassing sphere is:

$$\frac{V_O}{V_{\text{sphere}}} = \frac{(4/3)r^3}{(4/3)\pi r^3} = \frac{1}{\pi} = 0.318. \quad (\text{A.19})$$

Normalising the volume to that of a sphere of radius, a_{nd} we have

$$\frac{4}{3}\pi a_{\text{nd}}^3 = \frac{4}{3} r_{\text{eff}}^3 \quad (\text{A.20})$$

and

$$r_{\text{eff}} = \pi^{1/3} a_{\text{nd}} = 1.465 a_{\text{nd}}. \quad (\text{A.21})$$

Appendix A.4: Regular truncated octahedral (tO) particles

Our attention now turns to a common nano-diamond particle shape, a regular truncated octahedron (e.g. Barnard & Sternberg 2005), an octahedron with its six vertices truncated into square $\{100\}$ facets, with a total edge length of $36l$ (see Fig. 1 and Tables 1 and 2) and an encompassing sphere of radius $r = \sqrt{(5/2)}l = 1.581l$. The surface of a truncated octahedron is comprised of eight hexagonal $\{111\}$ facets (each of area $3\sqrt{3}/2l^2$) and six square $\{100\}$ facets (each of area l^2) is:

$$\begin{aligned} A_{tO} &= 8 \left(\frac{3\sqrt{3}}{2} \right) l^2 + 6l^2 = 6(2\sqrt{3} + 1)l^2 \\ &= \frac{12(2\sqrt{3} + 1)}{5} r^2 = 10.714 r^2. \end{aligned} \quad (\text{A.22})$$

²¹ For regular octahedral particles there are only six CH₂ groups present, one to be found on each of the particle vertices.

Here the surface is in hexagonal $\{111\}$ facets, with $f_{s\{111\}} = 0.776$, and square $\{100\}$ facets, with $f_{s\{100\}} = 0.224$. In truncated octahedral particles both $\{111\}/\{111\}$ and $\{111\}/\{100\}$ edges exist (see Fig. 1). $\{111\}/\{111\}$ edges are alternating CH-terminated and an integral part of $\{111\}$ facets, while $\{111\}/\{100\}$ edges are CH₂-terminated and form part of the $\{100\}$ facets. The ratio of the total edge length, $E_{tO} = 36l = 36\sqrt{(2/5)}r = 22.768r$, to the total surface area of the particle is

$$\frac{E_{tO}}{A_{tO}} = \frac{36l}{6(2\sqrt{3} + 1)l^2} = \frac{6}{(2\sqrt{3} + 1)l} = \frac{3\sqrt{2}\sqrt{5}}{(2\sqrt{3} + 1)r} = \frac{2.125}{r}. \quad (\text{A.23})$$

The ratio of the surface area to that of an encompassing sphere is

$$\frac{A_{tO}}{A_{\text{sphere}}} = \frac{(12/5)(2\sqrt{3} + 1)r^2}{4\pi r^2} = \frac{3(2\sqrt{3} + 1)}{5\pi} = 0.853. \quad (\text{A.24})$$

The volume of a truncated octahedron is given by:

$$V_{tO} = 8\sqrt{2}l^3 = 8\sqrt{2}[\sqrt{(2/5)}r]^3 = \frac{32}{5\sqrt{5}}r^3 = 2.862r^3 \quad (\text{A.25})$$

and its volume with respect to that of an encompassing sphere of the same radius r is:

$$\frac{V_{tO}}{V_{\text{sphere}}} = \frac{[32/(5\sqrt{5})]r^3}{(4/3)\pi r^3} = \frac{24}{\pi 5\sqrt{5}} = 0.683. \quad (\text{A.26})$$

Normalising to the volume of a sphere with radius a_{nd} we have

$$\frac{4}{3}\pi a_{\text{nd}}^3 = \frac{32}{5\sqrt{5}} r_{\text{eff}}^3 \quad (\text{A.27})$$

and

$$r_{\text{eff}} = \left(\frac{\pi 5\sqrt{5}}{24} \right)^{1/3} a_{\text{nd}} = 1.135 a_{\text{nd}}. \quad (\text{A.28})$$

Appendix A.5: Regular cuboctahedral (cO) particles

Another common nano-diamond shape is the cuboctahedron with a total edge length of $24l$ (see Fig. 1 and Tables 1 and 2) and an encompassing sphere of radius $r = l$. The surface area of a cuboctahedron, which exhibits eight triangular $\{111\}$ facets (each of area $[\sqrt{3}/4]l^2$) and six square facets (each of area l^2) is:

$$A_{cO} = 8 \frac{\sqrt{3}}{4} l^2 + 6l^2 = 2(\sqrt{3} + 3)l^2 = 2(\sqrt{3} + 3)r^2 = 9.464 r^2. \quad (\text{A.29})$$

In cuboctahedral particles the surface is in triangular $\{111\}$ facets, with $f_{s\{111\}} = 0.366$, and square $\{100\}$ facets, with $f_{s\{100\}} = 0.634$. All edges are $\{111\}/\{100\}$ and equivalent (see Fig. 1) and their CH_{*n*} groups form an integral parts of their adjacent $\{111\}$ and $\{100\}$ facets. The ratio of the total edge length, $E_{cO} = 24l = 24r$, to the total surface area of such a particle is

$$\frac{E_{cO}}{A_{cO}} = \frac{24l}{2(\sqrt{3} + 3)l^2} = \frac{12}{(\sqrt{3} + 3)l} = \frac{12}{(\sqrt{3} + 3)r} = \frac{2.536}{r}. \quad (\text{A.30})$$

The ratio of the surface area of a cuboctahedron to that of its encompassing sphere is

$$\frac{A_{cO}}{A_{\text{sphere}}} = \frac{2(\sqrt{3} + 3)r^2}{4\pi r^2} = \frac{(\sqrt{3} + 3)}{2\pi} = 0.753. \quad (\text{A.31})$$

The volume of a cuboctahedron is given by:

$$V_{\text{CO}} = \frac{5\sqrt{2}}{3} l^3 = \frac{5\sqrt{2}}{3} r^3 = 2.357 r^3 \quad (\text{A.32})$$

and the ratio of its volume to that of the encompassing sphere of the same radius r is:

$$\frac{V_{\text{CO}}}{V_{\text{sphere}}} = \frac{5\sqrt{2/3} r^3}{(4/3)\pi r^3} = \frac{5\sqrt{2}}{4\pi} = 0.563 \quad (\text{A.33})$$

and normalising to a sphere of radius a_{nd}

$$\frac{4}{3}\pi a_{\text{nd}}^3 = \frac{5\sqrt{2}}{3} r_{\text{eff}}^3 \quad (\text{A.34})$$

the effective radius (r_{eff}) of a cuboctahedron with the same volume as a sphere of radius a_{nd} is then

$$r_{\text{eff}} = \left(\frac{4\pi}{5\sqrt{2}} \right)^{\frac{1}{3}} a_{\text{nd}} = 1.211 a_{\text{nd}}. \quad (\text{A.35})$$

Appendix A.6: Regular cube (C) particles

For geometrical completeness we here describe the properties of a regular cube, with a total edge length of $12l$ (see Fig. 1 and Tables 1 and 2) and an encompassing sphere of radius $r = \sqrt{3}/2 l = 0.866 l$. The surface area of a cube, comprised of six square $\{100\}$ facets of area l^2 , is:

$$A_{\text{C}} = 6l^2 = 8r^2. \quad (\text{A.36})$$

The ratio of the total edge length, $E_{\text{C}} = 12l = 24\sqrt{3}r$, to the total surface area is

$$\frac{E_{\text{C}}}{A_{\text{C}}} = \frac{12l}{6l^2} = \frac{2}{l} = \frac{\sqrt{3}}{r} = \frac{1.732}{r}. \quad (\text{A.37})$$

The ratio of the surface area of a cube to that of its encompassing sphere is

$$\frac{A_{\text{C}}}{A_{\text{sphere}}} = \frac{8r^2}{4\pi r^2} = \frac{2}{\pi} r = 0.637 r. \quad (\text{A.38})$$

The volume of the cube ($l^3 = 1.540 r^3$) with respect to that of an encompassing sphere of the same radius r is:

$$\frac{V_{\text{C}}}{V_{\text{sphere}}} = \frac{l^3}{(4/3)\pi r^3} = \frac{8/(3\sqrt{3}) r^3}{(4/3)\pi r^3} = \frac{2}{\pi\sqrt{3}} = 0.368. \quad (\text{A.39})$$

Normalising to the volume of a sphere with radius a_{nd} we have

$$\frac{4}{3}\pi a_{\text{nd}}^3 = \frac{8}{3\sqrt{3}} r_{\text{eff}}^3 \quad (\text{A.40})$$

and

$$r_{\text{eff}} = \left(\frac{\pi\sqrt{3}}{2} \right)^{\frac{1}{3}} a_{\text{nd}} = 1.396 a_{\text{nd}}. \quad (\text{A.41})$$

Appendix A.7: Regular truncated cube (tC) particles

In order to be fully complete we now describe a regular truncated cube, a cube with its eight vertices truncated into triangular facets, with a total edge length of $36l$ (see Fig. 1 and Tables 1 and 2) and an encompassing sphere of radius $r = \frac{1}{2}\sqrt{(7+4\sqrt{2})}l = 1.779l$. The surface of a truncated cube is thus comprised of eight triangular $\{111\}$ facets (each of area $\sqrt{3}/4 l^2$) and six octagonal $\{100\}$ facets (each of area $2[\sqrt{2}+1]l^2$) and its surface area is:

$$A_{\text{tC}} = 8 \frac{\sqrt{3}}{4} l^2 + 6[2(\sqrt{2}+1)] l^2 = 2[6(\sqrt{2}+1) + \sqrt{3}] l^2 \\ = \frac{8[6(\sqrt{2}+1) + \sqrt{3}]}{7+4\sqrt{2}} r^2 = 10.251 r^2. \quad (\text{A.42})$$

Here the surface is in triangular $\{111\}$ facets, with $f_{s\{111\}} = 0.107$, and octagonal $\{100\}$ facets, with $f_{s\{100\}} = 0.893$. The edges of truncated cube particles are $\{111\}/\{100\}$ and $\{100\}/\{100\}$ and their CH_n groupings an integral part of their adjacent facets. The ratio of the total edge length, $E_{\text{tC}} = 36l = 72/(\sqrt{7+4\sqrt{2}})r$, to the total surface area of such a particle is

$$\frac{E_{\text{tC}}}{A_{\text{tC}}} = \frac{36l}{2[6(\sqrt{2}+1) + \sqrt{3}] l^2} = \frac{3}{[(\sqrt{2}+1) + \sqrt{3}/6] l} \\ = \frac{3\sqrt{(7+4\sqrt{2})}}{2[(\sqrt{2}+1) + \sqrt{3}/6] r} = \frac{2.126}{r}. \quad (\text{A.43})$$

The ratio of the surface area of a truncated cube to that of its encompassing sphere is

$$\frac{A_{\text{tC}}}{A_{\text{sphere}}} = \frac{8[6(\sqrt{2}+1) + \sqrt{3}]/(7+4\sqrt{2}) r^2}{4\pi r^2} \\ = \frac{2[6(\sqrt{2}+1) + \sqrt{3}]}{\pi(7+4\sqrt{2})} = 0.816. \quad (\text{A.44})$$

The volume of the truncated cube is given by:

$$V_{\text{tC}} = \frac{7(3+2\sqrt{2})}{3} l^3 = \frac{56(3+2\sqrt{2})}{3[\sqrt{(7+4\sqrt{2})}]^3} r^3 = 2.416 r^3 \quad (\text{A.45})$$

and its volume with respect to that of an encompassing sphere of the same radius r is:

$$\frac{V_{\text{tC}}}{V_{\text{sphere}}} = \frac{56(3+2\sqrt{2})/\{3[\sqrt{(7+4\sqrt{2})}]^3\} r^3}{(4/3)\pi r^3} \\ = \frac{14(3+2\sqrt{2})}{\pi[\sqrt{(7+4\sqrt{2})}]^3} = 0.577. \quad (\text{A.46})$$

Normalising to the volume of a sphere with radius a_{nd} we have

$$\frac{4}{3}\pi a_{\text{nd}}^3 = \frac{56(3+2\sqrt{2})}{3[\sqrt{(7+4\sqrt{2})}]^3} r_{\text{eff}}^3 \quad (\text{A.47})$$

and

$$r_{\text{eff}} = \frac{\sqrt{(7+4\sqrt{2})} \pi^{\frac{1}{3}}}{[14(3+\sqrt{2})]^{\frac{1}{3}}} a_{\text{nd}} = 1.201 a_{\text{nd}}. \quad (\text{A.48})$$

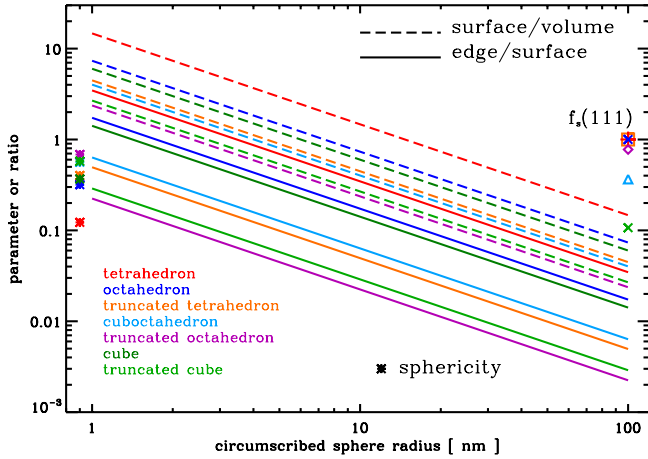


Fig. A.1. Spatial properties of regular polyhedra. The coloured dashed lines show the surface area to volume ratios of T (red), tT (orange), O (blue), tO (purple), cO (cobalt), C (dark green), and tC (green) particle forms, and the solid lines show the edge/surface area ratio. The asterisk symbols on the far left show their ‘sphericities’ and the different coloured symbols on the right indicate the fraction of the particle surface in {111} facets, which is zero for a cube (C).

Appendix A.8: The spatial properties of regular polyhedra

In the preceding sub-sections we described the surface and volume properties of known and other possible nano-diamond polyhedral forms. Fig. A.1 shows the surface area to volume ratios of T (red), tT (orange), O (blue), tO (purple), and cO (cobalt) particle forms (dashed lines), and their edge/surface area ratios (solid lines). Also shown are their ‘sphericities’ (asterisks on the left), the ratio of the volume of the polyhedron to that of its circumscribed sphere, and the surface fraction in {111} facets, $f_{s\{111\}}$ (different shaped and coloured symbols on the right, these data also appear in Fig. 1).

Given that the primary motivation for this study is to better understand the [CH]/[CH₂] abundance ratio on nano-diamond surfaces and the associated 3.53 μm(CH)/3.43 μm(CH₂) IR band intensity ratio, perhaps the most interesting result in Fig. A.1 is the wide variation in the CH-covered, {111} facet surface fraction, $f_{s\{111\}}$. For each of the seven regular polyhedra considered in this study $f_{s\{111\}}$ is independent of size and spreads over almost an order of magnitude (0.107 – 1.000). Nevertheless, $f_{s\{111\}}$ is not a good indication of the surface CH_n composition because it does not take account disproportionate edge effects.

Other things to note in Fig. A.1 are that: the particle ‘sphericity’ roughly increases with the number of polyhedral faces, that is particle complexity, and the surface-to-volume and edge-to-surface ratios decrease linearly in a log-log plot with increasing size.

Appendix B: Semi-regular polyhedral particles

We now consider the more complex case of semi-regularly truncated polyhedra with truncated facets that are of arbitrary size, which remain parallel to those of the regularly truncated parent polyhedron. In this case the expressions are necessarily more cumbersome and cannot be reduced to relatively straightforward expressions of, r , the radius of the sphere that circum-

scribes the particle and includes all its vertices.²² The truncated facet edges are assumed to be of arbitrary length a , which implies that the remnant edge, L , of the regular polyhedron parent is reduced from l to $(l - 2a)$ as illustrated in Figs. 3 to 5, that is $L = (l - 2a)$.

As will become clear in the following sections, for the expressions to hold in the case of each of the three truncated polyhedra that we consider, the following condition must hold

$$\frac{a}{l} \leq \frac{1}{2}, \quad (\text{B.1})$$

that is the parent polyhedron edge length is maximally-truncatable at its centre and we note that when

$a = 0$ ($\equiv L = l$) \rightarrow a regular parent polyhedron,

$a = l/3$ ($\equiv L = a$) \rightarrow a regular truncated parent polyhedron,

$a = l/2$ ($\equiv L = 0$) \rightarrow a different polyhedron. (B.2)

In the $L = 0$ case the truncated tetrahedron solution is an octahedron, and for a truncated octahedron or cube the solution is a cuboctahedron.

Appendix B.1: Semi-regular truncated tetrahedral (stT) particles

These are similar to truncated tetrahedral particles except that the four vertices are now arbitrarily truncated into equal equilateral triangular faces of edge length a (see Fig. 3). The total edge length is now $12a + 6(l - 2a) = 6l$, that is truncation does not change the total edge length compared to the parent tetrahedron. In this case the encompassing sphere radius is

$$r = \left(\frac{3}{8}L^2 + \frac{1}{2}aL + \frac{1}{2}a^2 \right)^{\frac{1}{2}}, \quad (\text{B.3})$$

where $L = (l - 2a)$, and which gives the values for the regular tetrahedron, truncated tetrahedron, and octahedron for $a = 0$, $a = L$, and $L = 0$, respectively. The above equation can, for later convenience, be re-arranged as a function of the remnant edge length L and the edge length ratio (a/L), to

$$r = L \left\{ \frac{3}{8} + \frac{1}{2} \left(\frac{a}{L} \right) + \frac{1}{2} \left(\frac{a}{L} \right)^2 \right\}^{\frac{1}{2}}. \quad (\text{B.4})$$

The surface area of a semi-regular truncated tetrahedron, with four equivalent, triangular {111} facets, each of area $\sqrt{3}/4 a^2$, and four six-sided facets, each of area $\sqrt{3}/4 (l^2 - 3a^2)$, is:

$$A_{stT} = \sqrt{3} (l^2 - 2a^2). \quad (\text{B.5})$$

In this case $a = l/2$ leads to a singularity and so we instead set $a = 0.49l$ in order to provide indicative data points for this limiting case in the figures. Given that the entire surface area is in triangular and six-sided {111} facets, $f_{s\{111\}} = 1$. However, as noted above for tT polyhedra, not all edges are of {100} CH₂-type, only 6 are and hence $E_{\{100\}} = 6L$. The ratio of the total edge length, E_{stT} , to the total surface area is

$$\frac{E_{stT}}{A_{stT}} = \frac{6l}{\sqrt{3}(l^2 - 2a^2)} = \frac{2\sqrt{3}l}{(l^2 - 2a^2)} \quad (\text{B.6})$$

²² However, all particles can still be circumscribed by an all-vertex encompassing sphere of radius r .

and the ratio of the surface area to that of the encompassing sphere is

$$\frac{A_{\text{stT}}}{A_{\text{sphere}}} = \frac{\sqrt{3}(l^2 - 2a^2)}{4\pi r^2} = \frac{\sqrt{3}(l^2 - 2a^2)}{4\pi \left(\frac{3}{8}L^2 + \frac{1}{2}aL + \frac{1}{2}a^2\right)}. \quad (\text{B.7})$$

The volume of a semi-regular truncated tetrahedron is given by:

$$V_{\text{stT}} = \frac{\sqrt{2}}{12}(l^3 - 4a^3) \quad (\text{B.8})$$

and the ratio of the volume of a semi-regular truncated tetrahedron (radius r) to that of its encompassing sphere of the same radius r is:

$$\frac{V_{\text{stT}}}{V_{\text{sphere}}} = \frac{\frac{\sqrt{2}}{12}(l^3 - 4a^3)}{\frac{4}{3}\pi r^3} = \frac{\sqrt{2}(l^3 - 4a^3)}{16\pi \left(\frac{3}{8}L^2 + \frac{1}{2}aL + \frac{1}{2}a^2\right)^{\frac{3}{2}}}. \quad (\text{B.9})$$

Equating V_{stT} to a spherical particle of the same volume to determine the radius, a_{nd} , of the equivalent "spherical nano-diamond" we have

$$\frac{4}{3}\pi a_{\text{nd}}^3 = \frac{\sqrt{2}}{12}(l^3 - 4a^3). \quad (\text{B.10})$$

This expression is not directly solvable for r_{eff} as for regular polyhedra and so we need to adopt a different approach. Substituting $l = (L + 2a)$ and re-arranging the above equation to the following form we have

$$L_{\text{eff}} = \left\{ \frac{\pi 8\sqrt{2}}{1 + 6(a/L) + 12(a/L)^2 + 4(a/L)^3} \right\}^{\frac{1}{3}} a_{\text{nd}}, \quad (\text{B.11})$$

where the ratio (a/L) is defined for the particular truncated particle shape under consideration.²³ We can determine the remnant polyhedron effective edge length, L_{eff} , and substitute this and (a/L) into Eq. (B.4) and thus obtain the value of r_{eff} that corresponds to the required nano-diamond radius a_{nd} . Alternatively we can bypass r_{eff} and calculate a_{nd} directly by solving Eq. (B.10), that is

$$a_{\text{nd}} = \left\{ \frac{\sqrt{2}}{16\pi}(l^3 - 4a^3) \right\}^{\frac{1}{3}}. \quad (\text{B.12})$$

Appendix B.2: Semi-regular truncated octahedral (stO) particles

These are octahedral particles with the six vertices arbitrarily truncated into equal square faces of edge length a . The total edge length is now $24a + 12(l - 2a) = 12l$, that is truncation does not change the total edge length with respect to the parent octahedron (see Fig. 4). The encompassing sphere radius is

$$r = \left(\frac{1}{2}L^2 + aL + a^2 \right)^{\frac{1}{2}}, \quad (\text{B.13})$$

where $L = (l - 2a)$, and which gives the values for the regular octahedron, truncated octahedron and cuboctahedron for $a = 0$, $a = L$, and $L = 0$, respectively. As above, and for later convenience, the above equation can be re-arranged as a function of the remnant edge length L and the edge length ratio (a/L) , to

$$r = L \left\{ \frac{1}{2} + \frac{a}{L} + \left(\frac{a}{L} \right)^2 \right\}^{\frac{1}{2}}. \quad (\text{B.14})$$

²³ N.B., (a/L) can take any positive value: for $a = 0$, $a = L$, and $L = 0$ we have $(a/L) = 0, 1$ and ∞ , respectively.

The surface area of a semi-regular truncated octahedron, with six equivalent, square $\{100\}$ facets, each of area a^2 , and eight six-sided $\{111\}$ facets, each of area $\sqrt{3}/4(l^2 - 3a^2)$, is:

$$A_{\text{stO}} = 8\frac{\sqrt{3}}{4}\sqrt{3}(l^2 - 3a^2) + 6a^2 = 2\left\{\sqrt{3}l^2 - 3(\sqrt{3} - 1)a^2\right\}. \quad (\text{B.15})$$

The fraction of the surface in $\{111\}$ facets, $f_{s\{111\}}$, is

$$f_{s\{111\}} = \frac{2\sqrt{3}(l^2 - 3a^2)}{2\sqrt{3}(l^2 - 3a^2) + 6a^2} = \left\{ \frac{1 - 3(a/l)^2}{1 - (3 - \sqrt{3})(a/l)^2} \right\} \quad (\text{B.16})$$

and, trivially, $f_{s\{100\}} = (1 - f_{s\{111\}})$. The square truncated facet edges, of total length $24a$, are of $\{100\}$ -type and are therefore included in the $\{100\}$ facet CH_2 groups. However, the twelve edges of length $L = (l - 2a)$ of the six-sided faces are $\{111\}/\{111\}$ edges, hence $E_{\{111\}} = 12L = 12(l - 2a)$, and their CH groups form part of the adjacent $\{111\}$ facets. The ratio of the total edge length, E_{stO} , to the total surface area is

$$\frac{E_{\text{stO}}}{A_{\text{stO}}} = \frac{12l}{2\left\{\sqrt{3}l^2 - 3(\sqrt{3} - 1)a^2\right\}} = \left\{ \frac{\sqrt{3}}{6}l - \frac{1}{2}(\sqrt{3} - 1)\frac{a^2}{l} \right\}^{-1} \quad (\text{B.17})$$

and the ratio of the surface area to that of the encompassing sphere is

$$\frac{A_{\text{stO}}}{A_{\text{sphere}}} = \frac{2\left\{\sqrt{3}l^2 - 3(\sqrt{3} - 1)a^2\right\}}{4\pi r^2} = \frac{\sqrt{3}l^2 - 3(\sqrt{3} - 1)a^2}{2\pi \left(\frac{1}{2}L^2 + aL + a^2\right)}. \quad (\text{B.18})$$

The volume of a semi-regular truncated octahedron is given by:

$$V_{\text{stO}} = \frac{\sqrt{2}}{3}(l^3 - 3a^3) \quad (\text{B.19})$$

and the ratio of its volume (radius r) to that of its encompassing sphere of the same radius r is:

$$\frac{V_{\text{stO}}}{V_{\text{sphere}}} = \frac{\frac{\sqrt{2}}{3}(l^3 - 3a^3)}{\frac{4}{3}\pi r^3} = \frac{\sqrt{2}(l^3 - 3a^3)}{4\pi \left(\frac{1}{2}L^2 + aL + a^2\right)^{\frac{3}{2}}}. \quad (\text{B.20})$$

Equating V_{stO} to a spherical particle of the same volume to determine the radius, a_{nd} , of the equivalent 'spherical nano-diamond' we have

$$\frac{4}{3}\pi a_{\text{nd}}^3 = \frac{\sqrt{2}}{3}(l^3 - 3a^3). \quad (\text{B.21})$$

This expression is not directly solvable for r_{eff} as for regular polyhedra and so as in the preceding case we substitute $l = (L + 2a)$ and re-arrange to the following form

$$L_{\text{eff}} = \left\{ \frac{\pi 2\sqrt{2}}{1 + 6(a/L) + 12(a/L)^2 + 5(a/L)^3} \right\}^{\frac{1}{3}} a_{\text{nd}}, \quad (\text{B.22})$$

where the ratio (a/L) is defined for the particular truncated particle shape under consideration. We can determine the remnant polyhedron effective edge length, L_{eff} , and substitute this and (a/L) into Eq. (B.14) and thus obtain the value of r_{eff} that corresponds to the required nano-diamond radius a_{nd} . Again, if we do not need r_{eff} , we can calculate a_{nd} by solving Eq. (B.21), that is

$$a_{\text{nd}} = \left\{ \frac{\sqrt{2}}{4\pi}(l^3 - 3a^3) \right\}^{\frac{1}{3}}. \quad (\text{B.23})$$

Appendix B.3: Semi-regular truncated cubic (stC) particles

These are cubes with the eight vertices arbitrarily truncated into equilateral triangular faces of edge length a . The total edge length is now $24a + 12[l - \sqrt{2}a] = [12l + 12a(2 - \sqrt{2})]$ (see Fig. 5). Note that in this case truncation does change the total edge length with respect to the parent cube. The encompassing sphere radius is

$$r = \left(\frac{3}{4}L^2 + \sqrt{2}aL + a^2 \right)^{\frac{1}{2}}, \quad (\text{B.24})$$

where $L = (l - 2a)$, and which gives the values for the regular cube, truncated cube and cuboctahedron for $a = 0$, $a = L$, and $L = 0$, respectively. Once again for later convenience we re-arrange the above equation as a function of the remnant edge length L and the edge length ratio (a/L), to

$$r = L \left\{ \frac{3}{4} + \sqrt{2} \frac{a}{L} + \left(\frac{a}{L} \right)^2 \right\}^{\frac{1}{2}}. \quad (\text{B.25})$$

The surface area of an semi-regular truncated cube, with eight equivalent, triangular $\{111\}$ facets, each of area $(\sqrt{3}/4)a^2$, and six eight-sided $\{100\}$ facets, each of area $(l^2 - a^2)$, is:

$$A_{\text{stC}} = 8(\sqrt{3}/4)a^2 + 6(l^2 - a^2) = 6l^2 + 2(\sqrt{3} - 3)a^2. \quad (\text{B.26})$$

The fraction of the surface in $\{111\}$ facets, $f_{s\{111\}}$, is

$$f_{s\{111\}} = \frac{8(\sqrt{3}/4)a^2}{6l^2 + 2(\sqrt{3} - 3)a^2} = \sqrt{3} \left\{ 3 \left(\frac{l}{a} \right)^2 + \sqrt{3} - 6 \right\}^{-1} \quad (\text{B.27})$$

and, trivially, $f_{s\{100\}} = (1 - f_{s\{111\}})$. The triangular truncated $\{111\}$ facet edges, of total length $24a$, all border $\{100\}$ facets are of $\{100\}$ -type and their CH₂ groups are therefore included in the $\{100\}$ facets. All other edges are $\{100\}/\{100\}$ edges, hence $E_{\{111\}} = 0$. The ratio of the total edge length, E_{stC} , to the total surface area is

$$\frac{E_{\text{stC}}}{A_{\text{stC}}} = \frac{[12l + 12a(2 - \sqrt{2})]}{6l^2 + 2(\sqrt{3} - 3)a^2} = \frac{2[(l/a) + 2 - \sqrt{2}]}{(l^2/a) + (\sqrt{3}/3 - 1)a} \quad (\text{B.28})$$

and the ratio of the surface area to that of the encompassing sphere is

$$\begin{aligned} \frac{A_{\text{stC}}}{A_{\text{sphere}}} &= \frac{6l^2 + 2(\sqrt{3} - 3)a^2}{4\pi r^2} = \frac{6l^2 + 2(\sqrt{3} - 3)a^2}{4\pi \left(\frac{3}{4}L^2 + \sqrt{2}aL + a^2 \right)} \\ &= \frac{(l/a)^2 + \sqrt{3}/3 - 1}{\frac{2}{3}\pi \left[\frac{3}{4}(L/a)^2 + \sqrt{2}(L/a) + 1 \right]}. \end{aligned} \quad (\text{B.29})$$

The volume of a semi-regular truncated cube is given by:

$$V_{\text{stC}} = \frac{1}{3}(3l^3 - \sqrt{2}a^3) \quad (\text{B.30})$$

and the ratio of its volume (radius r) to that of its encompassing sphere of the same radius r is:

$$\frac{V_{\text{stC}}}{V_{\text{sphere}}} = \frac{\frac{1}{3}(3l^3 - \sqrt{2}a^3)}{\frac{4}{3}\pi r^3} = \frac{(3l^3 - \sqrt{2}a^3)}{4\pi \left(\frac{3}{4}L^2 + \sqrt{2}aL + a^2 \right)^{\frac{3}{2}}}. \quad (\text{B.31})$$

Equating V_{stC} to a spherical particle of the same volume to determine the radius, a_{nd} , of the equivalent "spherical nano-diamond" we have

$$\frac{4}{3}\pi a_{\text{nd}}^3 = \frac{1}{3}(3l^3 - \sqrt{2}a^3). \quad (\text{B.32})$$

Once again we have an equation that is not directly solvable for r_{eff} and so we substitute $l = (L + 2a)$ and re-arrange to the following

$$L_{\text{eff}} = \left\{ \frac{4\pi}{3[1 + 6(a/L) + 12(a/L)^2 + (8 + \sqrt{2}/3)(a/L)^3]} \right\}^{\frac{1}{3}} a_{\text{nd}}, \quad (\text{B.33})$$

where the ratio (a/L) is defined for the particular truncated particle shape under consideration. This again allows us to determine the remnant polyhedron effective edge length, L_{eff} , and substitute this and (a/L) into Eq. (B.25) and thus obtain the value of r_{eff} that corresponds to the required nano-diamond radius a_{nd} . Again we can bypass r_{eff} and calculate a_{nd} by solving Eq. (B.32), that is

$$a_{\text{nd}} = \left\{ \frac{1}{4\pi}(3l^3 - \sqrt{2}a^3) \right\}^{\frac{1}{3}}. \quad (\text{B.34})$$